INSTITUTE OF PHYSICS PUBLISHING INVERSE PROBLEMS

Inverse Problems **20** (2004) 753–780 PII: S0266-5611(04)74299-9

Magnetic resonance imaging in inhomogeneous fields

Charles L Epstein

Department of Mathematics, University of Pennsylvania, Philadelphia, PA, USA
and
LSNI, Hospital of the University of Pennsylvania, Philadelphia, PA, USA

E-mail: cle@math.upenn.edu

Received 8 January 2004, in final form 1 March 2004
Published 19 March 2004
Online at stacks.iop.org/IP/20/753 (DOI: 10.1088/0266-5611/20/3/007)

Abstract

In this paper, we explain the principles underlying imaging with an inhomogeneous $\boldsymbol{B}_0$-field and show how SNR and SAR considerations place limits on the size of the relative field inhomogeneity. We explore problems of imaging with a background field that varies in both magnitude and direction, both with and without critical points. We give a simple geometric explanation for the difficulties that arise when attempting to use fields such that $\|\widehat{\boldsymbol{B}}_0\|$ has a saddle point, and construct examples of fields where $\|\widehat{\boldsymbol{B}}_0\|$ has isolated, nonzero minima.

(Some figures in this article are in colour only in the electronic version)

1. Introduction

In the standard approach to magnetic resonance imaging one uses a strong background field that is as homogeneous as possible. Commercial MR imaging magnets are homogeneous, within the field of view, to about 10 ppm. In 'open' MRI systems, the field homogeneity is somewhat less, but still in this general range. One can imagine a variety of situations where it might be useful to do magnetic resonance imaging with the object placed entirely *outside* the magnet's bore. As a consequence of Runge's theorem, it is possible to design coils so that this external field is as homogeneous as one would like, in a given region of space. However, this requires a large expenditure of power and complicated, difficult to design arrangements of coils, see [19, 20]. On the other hand with very simple arrangements of permanent magnets or electromagnets one can produce a field, $\widehat{\boldsymbol{B}}_0$, such that, in a given region of space, exterior to the magnets or coils (1) the field is strong, (2) the direction of $\widehat{\boldsymbol{B}}_0$ varies in a small solid angle, (3) the level sets of $\|\widehat{\boldsymbol{B}}_0\|$ are smooth, (4) the size of $\nabla\|\widehat{\boldsymbol{B}}_0\|$ is not too large. In this paper we explore the problems connected to imaging in such a field.

We consider three problems which arise in imaging: (1) excitation, (2) spatial encoding and (3) image reconstruction. There are, of course, many other issues that would arise in the

practical implementation of such an imaging system. This paper is of a theoretical character, and the analysis of these more practical problems will have to wait for experimental work.

First of all, what do we mean by 'imaging in an inhomogeneous background field'? Because the local resonance frequency is determined by the magnitude of the local field, small variations in $\|\boldsymbol{B}_0\|$ are of much greater importance than small variations in its direction. We are imaging in an inhomogeneous background field if $\nabla\|\widehat{\boldsymbol{B}}_0\|$ has a 'large,' time-*independent* component throughout the imaging experiment. We are not considering the sorts of 'random' or localized inhomogeneities which arise from the physical properties of the object being imaged, e.g. susceptibility artefacts. At the outset, the problem of imaging with an inhomogeneous background field splits into two cases:

Noncritical case. The function $\|\widehat{\boldsymbol{B}}_0\|$ has no critical points in the field of view, the level sets of $\|\widehat{\boldsymbol{B}}_0\|$ are smooth, and fit together nicely.

Critical case. The function $\|\widehat{\boldsymbol{B}}_0\|$ has critical points within the field of view.

The techniques available for spatial localization are different in each case, and we treat them separately.

The first problems that one encounters are connected to selective excitation. Because the permanent gradient tends to be large, a large RF-bandwidth may be required to excite a sufficiently wide slice. Beyond this bandwidth problem, one might also expect small variations in the direction of $\widehat{\boldsymbol{B}}_0$ to lead to difficulties with selective excitation. However, this turns out to be a relatively minor problem. As explained in appendix A, if the direction of $\widehat{\boldsymbol{B}}_0$ does not vary too much, then a selective RF-pulse sequence excites spins lying in a region of space of the form

$$\{(x, y, z) : \omega_0 - \Delta\omega \leqslant \gamma\|\widehat{\boldsymbol{B}}_0(x, y, z)\| \leqslant \omega_0 + \Delta\omega\}. \tag{1}$$

If $\nabla\|\widehat{\boldsymbol{B}}_0\|$ does not vanish within this set then the selected slice is a nonlinear analogue of the region between two planes, see figure 5. In this paper, we also consider the case that the level set

$$\mathscr{S}_{\omega_0} = \{(x, y, z) : \gamma\|\widehat{\boldsymbol{B}}_0(x, y, z)\| = \omega_0\} \tag{2}$$

contains a single isolated critical point.

We begin with the noncritical case. In the approach we describe below, the permanent gradient in $\widehat{\boldsymbol{B}}_0$ is used as a slice select gradient. The problem of imaging in a noncritical, inhomogeneous field becomes, at least conceptually, the problem of imaging with a permanent slice select gradient. So as not to confuse the reader, we emphasize that this is not an imposed gradient, which could be reversed, but rather a permanent and irreversible gradient that arises from the basic design of the imaging system and the placement of the sample. In the noncritical case, we obtain conditions on the background field so that the measured signal can, up to appropriate changes in variable, be regarded as samples of a Fourier transform. In principle, the needed changes of variable can be computed with a knowledge of the background field and the gradient fields throughout the field of view. Our principal observation in this regard is that, so long as the direction of $\widehat{\boldsymbol{B}}_0$ does not vary too much within the field of view, the most important property for the imaging system is to have a two-parameter *linear family* of gradient fields. The gradients themselves need not be linear. This is explained in detail in section 3.

In order to have a concrete example in mind we consider the following situation: imagine that we have two infinite, concentric arcs of cylinders with current running in opposite directions, along their axes. The field of view is a region outside both arcs. The set-up is shown in figure 1. With infinitely long cylinders, the field is independent of the z-coordinate and lies in the xy-plane. Figure 2(a) shows level lines of the field generated by the apparatus in

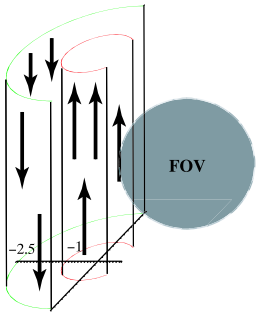

Figure 1. An electromagnet constructed out of two concentric cylindrical segments. The inner cylinder subtends 270°, the outer cylinder subtends 180°. The current on the inner cylinder is 0.6 units and that on the outer cylinder is 2 units. As indicated, the FOV is a region of space exterior to the arcs of both cylinders.

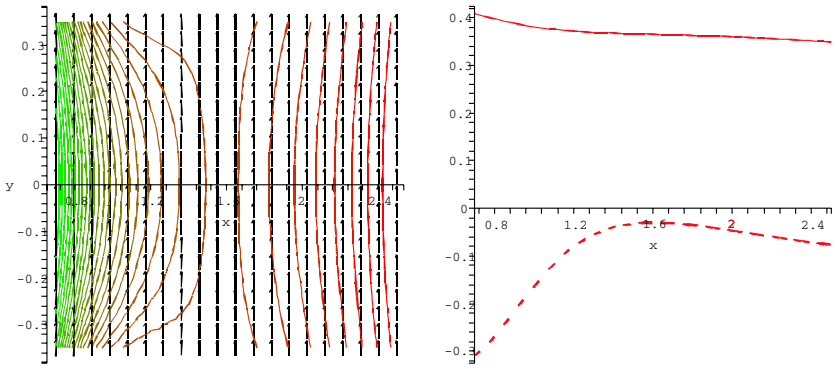

(a) (b)

Figure 2. Properties of the magnetic field generated by the arrangement of conductors shown in figure 1. The inner current is 0.6 units and the outer current is 2 units. (a) Level contours of $\|\widehat{\boldsymbol{B}}_0\|$ and field vectors (the essentially vertical lines). (b) Plot of $\|\widehat{\boldsymbol{B}}_0\|$ (solid line) and $\nabla\|\widehat{\boldsymbol{B}}_0\|/\|\widehat{\boldsymbol{B}}_0\|$ (dashed line) along $y = 0$.

figure 1, along with vectors indicating its local direction. Figure 2(b) shows the field strength (solid line), and the relative gradient (dashed line) $\nabla\|\widehat{\boldsymbol{B}}_0\|/\|\widehat{\boldsymbol{B}}_0\|$, along the y-axis

At each point (x, y, z), the direction of the background field, $\widehat{\boldsymbol{B}}_0(x, y, z)$, defines a 'local z-direction'. The transverse component of the magnetization at (x, y, z) is the part of the magnetization orthogonal to $\widehat{\boldsymbol{B}}_0(x, y, z)$. This component of the magnetization precesses about $\widehat{\boldsymbol{B}}_0(x, y, z)$ at the *local Larmor frequency*, which equals $\gamma\|\widehat{\boldsymbol{B}}_0(x, y, z)\|$. As the definition of the 'rotating reference frame' varies from point to point, we often work in the laboratory reference frame.

For the purposes of our discussion, we refer to the perturbations of $\widehat{\boldsymbol{B}}_0$, used for spatial encoding (i.e. gradients), as 'time-independent' fields. Such fields are typically turned on for a period of time, and then turned off, and so are not, strictly speaking, time independent. We wish to distinguish them from the RF-fields used for selective excitation. The RF-fields vary on the time scale of the Larmor period. The reason for this distinction is that, so long as $\widehat{\boldsymbol{B}}_0$ is a very strong field, the important component of a 'time-independent' field is the component parallel to $\widehat{\boldsymbol{B}}_0$, whereas the important components of an RF-field are those orthogonal to $\widehat{\boldsymbol{B}}_0$.

Throughout this paper we assume that the $\widehat{\boldsymbol{B}}_0$-field is strong enough that the components of gradient fields, in directions orthogonal to it, can safely be ignored.

We use $\boldsymbol{B}_0$ to denote magnetic fields in the direction of $\widehat{\boldsymbol{B}}_0$. In most applications of MR it is only the spatial dependence of the magnitude of $\boldsymbol{B}_0$ which is carefully accounted for. Indeed, it is usually assumed that the gradients are 'linear' so that (in standard homogeneous field imaging)

$$\widehat{\boldsymbol{B}}_0 = b_0\hat{\boldsymbol{z}} \qquad \boldsymbol{B}_0(x, y, z) = \widehat{\boldsymbol{B}}_0 + (x, y, z)\cdot(g_x, g_y, g_z)\hat{\boldsymbol{z}}. \tag{3}$$

The linear function $(x, y, z)\cdot(g_x, g_y, g_z)$ (or sometimes the vector (g_x, g_y, g_z) itself) is called the 'gradient'. It is the projection of a *gradient field* in the direction of $\widehat{\boldsymbol{B}}_0$. In the inhomogeneous case we need to be a bit more careful, and so we work with magnetic fields which generate the gradients. If $\boldsymbol{G}$ is such a gradient field then the perturbed background field is given by

$$\boldsymbol{B}_0 = \widehat{\boldsymbol{B}}_0 + \frac{\widehat{\boldsymbol{B}}_0\cdot\boldsymbol{G}}{\|\widehat{\boldsymbol{B}}_0\|}\frac{\widehat{\boldsymbol{B}}_0}{\|\widehat{\boldsymbol{B}}_0\|}. \tag{4}$$

As noted above, the components of $\boldsymbol{G}$ orthogonal to $\widehat{\boldsymbol{B}}_0$ have very little effect on the evolution of spins.

In the MR-literature, a point where $\nabla\|\widehat{\boldsymbol{B}}_0\|$ vanishes is sometimes called a 'sweet spot'. Following the usual practice in the mathematics literature, we call such a point a *critical point* of $\|\widehat{\boldsymbol{B}}_0\|$. The value of $\|\widehat{\boldsymbol{B}}_0\|$ at a critical point is called a *critical value* of $\|\widehat{\boldsymbol{B}}_0\|$. We normalize coordinates so that the critical point is located at $(0, 0, 0)$ and let ω_0 denote the critical value, $\gamma\|\widehat{\boldsymbol{B}}_0(0, 0, 0)\|$. The geometry of the level sets $\mathscr{S}_\omega$, for values of ω near to ω_0, is determined by the nature of the critical point that $\|\widehat{\boldsymbol{B}}_0\|$ has at $(0, 0, 0)$. Because the components of $\widehat{\boldsymbol{B}}_0$ are harmonic functions, the function $\|\widehat{\boldsymbol{B}}_0(x, y, z)\|$ is subharmonic. The maximum principle implies that $\|\widehat{\boldsymbol{B}}_0\|$ cannot have a local maximum value, see [4]. Thus $(0, 0, 0)$ can be either a saddle point or a local minimum. So far as I am aware, the only case that has been considered in the literature is that of a saddle point. We consider this case and give a new explanation as to why this is a problematic geometry for imaging. We also construct examples to show that magnetic fields exist such that $\|\widehat{\boldsymbol{B}}_0\|$ attains a nonzero local minimum value. These fields provide new opportunities for localized spectroscopy, which are not available in earlier approaches of this sort, e.g. FONAR and TOPICAL, see [7] and [13]. In particular, with each acquisition one can measure a complete FID generated by the material located in a single pixel.

In sections 2 and 3 we consider the measurement process for background fields without critical points within the field of view. In section 4, we show how considerations of SNR and SAR put bounds on the size of $\|\nabla\|\widehat{\boldsymbol{B}}_0\|\|/\|\widehat{\boldsymbol{B}}_0\|$. In section 5 we consider the local geometry of the level sets of a function of three variables, with an isolated critical point, and introduce the concept of Morse coordinates. In section 6 we explore the difficulties associated with attempts to image using a field with an isolated saddle point, and in section 7 we show how to construct fields so that $\|\widehat{\boldsymbol{B}}_0\|$ has an isolated minimum value. In appendix A we show that the process of selective excitation is relatively insensitive to the angle between the $\boldsymbol{B}_0$ and $\boldsymbol{B}_1$ fields. Finally, in appendix B, we demonstrate that the length of an axially symmetric field cannot have an isolated minimum value.

Remark 1 (Notational convention)**.** If $\{\tilde{\boldsymbol{x}}, \tilde{\boldsymbol{y}}, \tilde{\boldsymbol{z}}\}$ is an orthonormal frame for $\mathbb{R}^3$, then we often use the notation $[w, u]$ (note the square brackets $[\cdot, \cdot]$), where w is a complex number and u is a real number, to denote the vector $\mathrm{Re}(w)\tilde{\boldsymbol{x}} + \mathrm{Im}(w)\tilde{\boldsymbol{y}} + u\tilde{\boldsymbol{z}}$. Which orthonormal frame is being used should be clear from the context.

We denote the Fourier transform of a function f by $\mathscr{F}(f)$.

2. Inhomogeneous fields without critical points: 1

Most approaches to magnetic resonance imaging in a homogeneous background field follow essentially the same sequence of steps:

(1) The sample is polarized in the uniform background field.
(2) Using a slice select gradient, the sample is selectively excited using an RF-pulse.
(3) By reversing the slice select gradient, or using a refocusing pulse, the excited magnetization is rephased.
(4) Using gradient fields, the excited magnetization is 'spatially encoded'.
(5) The signal is acquired, possibly with additional spatial encoding.

In this section, we consider the problem of imaging with an inhomogeneous background field without critical points. To begin our discussion we consider a simplified model, with a background field, $\widehat{\boldsymbol{B}}_0(x, y, z)$, of the form

$$\widehat{\boldsymbol{B}}_0(x, y, z) = (b_0 - Gz)\hat{\boldsymbol{z}} \tag{5}$$

for $z \in [-z_{\max}, z_{\max}]$. While G/b_0 may be large, per unit distance, the field of view is constrained so that $b_0 \pm Gz_{\max}$ is also assumed to be large. This means that $\widehat{\boldsymbol{B}}_0$ is large within the field of view, and therefore, slowly varying perturbing fields, orthogonal to $\widehat{\boldsymbol{B}}_0$, can safely be ignored. Placing coils around the sample we generate the gradients and RF-pulses needed to do imaging. Here we have assumed that the gradient in $\|\widehat{\boldsymbol{B}}_0\|$ is parallel to the direction of $\widehat{\boldsymbol{B}}_0$. This simplifies the discussion, a little, but is not necessary to do the analysis. A similar analysis also applies to fields which are not assumed to point in a fixed direction, provided $\|\widehat{\boldsymbol{B}}_0\|$ is large throughout the field of view, and $\nabla\|\widehat{\boldsymbol{B}}_0\|$ does not vanish. The general case is considered in the next section.

Remark 2. In this section we use the laboratory frame, $\{\hat{\boldsymbol{x}}, \hat{\boldsymbol{y}}, \hat{\boldsymbol{z}}\}$, with $\hat{\boldsymbol{z}}$ parallel to $\widehat{\boldsymbol{B}}_0$. Therefore we have

$$[a + \mathrm{i}b, c] \leftrightarrow a\hat{\boldsymbol{x}} + b\hat{\boldsymbol{y}} + c\hat{\boldsymbol{z}}, \tag{6}$$

with the complex number, $a + \mathrm{i}b$, representing the *transverse component* of the magnetization. The computations in this section are done in the resonance rotating reference frame defined by $b_0\hat{\boldsymbol{z}}$.

In our analysis of fields without critical points, we use the permanent gradient in $\widehat{\boldsymbol{B}}_0$ as a slice select gradient. Leaving the sample stationary in the background field produces an equilibrium magnetization, $\boldsymbol{M}_0(x, y, z)$, given by

$$\begin{aligned} &\boldsymbol{M}_0(x, y, z) = C(T)\rho'(x, y, z)\widehat{\boldsymbol{B}}_0(x, y, z), \\ &C(T) = \frac{1.0075}{T}\ \mathrm{A\ m^{-1}}\ \text{ for protons in water.} \end{aligned} \tag{7}$$

Here $\rho'(x, y, z)$ is the density of water protons at (x, y, z). As noted, the constant $C(T)$ is inversely proportional to T, the absolute temperature. To simplify notation we let ρ denote $C(T)\rho'$. A principal goal of MRI is the determination of the function $\rho(x, y, z)$. If $\|\widehat{\boldsymbol{B}}_0(x, y, z)\|$ varies considerably over the support of $\rho(x, y, z)$, then it may be necessary to include $\|\widehat{\boldsymbol{B}}_0(x, y, z)\|$ in the definition of the equilibrium magnetization. In this section we assume that this is not the case, and use b_0 to denote $\|\widehat{\boldsymbol{B}}_0(x, y, z)\|$ in the formula for the equilibrium magnetization.

In light of the permanent gradient, we do not have to 'turn on' the slice select gradient. While the Bloch equation analysis of selective excitation applies, essentially verbatim, a few

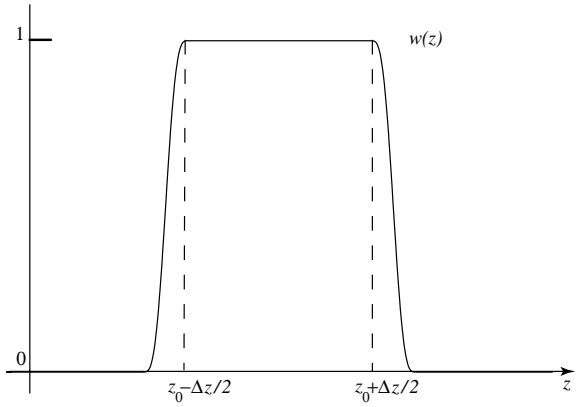

Figure 3. The graph of a typical normalized magnetization profile.

remarks are in order. If $\widehat{\boldsymbol{B}}_0$ always points in the same direction, as in (5), then the usual analysis from the homogeneous case applies without change. In general, the direction of $\widehat{\boldsymbol{B}}_0$ may vary slowly over the field of view. In this case, we can still use a selective RF-pulse designed for use with a $\widehat{\boldsymbol{B}}_0$-field having a permanent gradient, but uniform direction, as in equation (5). In appendix A we show that the main consequence of nonorthogonality between $\widehat{\boldsymbol{B}}_0$ and $\boldsymbol{B}_1$ is a decrease in the effective amplitude of $\boldsymbol{B}_1$. If the angle between $\widehat{\boldsymbol{B}}_0(x, y, z)$ and $\boldsymbol{B}_1(x, y, z; t)$ is $\frac{\pi}{2} + \phi$, then the effective RF-field at this point is $\frac{(1+\cos\phi)}{2}\boldsymbol{B}_1(x, y, z; t)$. Attenuating the RF slightly, diminishes the flip angle and introduces a small phase error, but has very little effect on the selectivity of the pulse, see figures 12 and 13. If, over the extent of the sample, the angle between $\boldsymbol{B}_1$ and $\widehat{\boldsymbol{B}}_0$ is close to $\frac{\pi}{2}$, then there will be some (removable) shading in the image. Hence, if $\boldsymbol{B}_1$ is designed to excite spins with offset frequencies in the band $[f_{\min}, f_{\max}]$, then the actual excited slice is given by the (nonlinear) region of space

$$\{(x, y, z) : \omega_0 + f_{\min} \leqslant \gamma \|\widehat{\boldsymbol{B}}_0(x, y, z)\| \leqslant \omega_0 + f_{\max}\}.$$

The slices are bounded by level sets of $\|\widehat{\boldsymbol{B}}_0(x, y, z)\|$.

The first significant difference between imaging in homogeneous fields and in inhomogeneous fields occurs at step 3. In the latter case, it is not possible to reverse the slice select gradient to rephase the magnetization after the application of a selective pulse. The only realistic options are to use a self-refocused pulse or a refocusing pulse. A self refocused pulse is only refocused once, so we do not consider this option further.

We apply a selective RF-pulse with normalized excitation profile as shown in figure 3. Assuming $\widehat{\boldsymbol{B}}_0$ is given by (5), then, at the end of a selective RF-pulse, the magnetization is given by

$$\boldsymbol{M}(x, y, z) = Cb_0\rho(x, y, z)\big[\exp(\mathrm{i}\gamma Gz\tau_1)w(z), \operatorname{sgn}(z)\sqrt{1 - w^2(z)}\big], \tag{8}$$

with τ_1 the rephasing time for the selective RF-pulse. The function $\operatorname{sgn}(z)$ takes the values ± 1; it is included to allow for flip angles larger than 90°. In general $\operatorname{sgn}(z) = 1$ for z outside a finite band. If we were to immediately apply a refocusing pulse, then, at its conclusion, the magnetization would be given by

$$\boldsymbol{M}(x, y, z) = Cb_0\rho(x, y, z)\big[\exp(-\mathrm{i}\gamma Gz\tau_1)w(z), \operatorname{sgn}(z)\sqrt{1 - w^2(z)}\big]. \tag{9}$$

Normalizing so that $t = 0$ at the conclusion of the refocusing pulse, the magnetization, as a function of space and time is given, for $t \geqslant 0$, by

$$\boldsymbol{M}'(x, y, z; t) = Cb_0\rho(x, y, z)\big[\exp(\mathrm{i}\gamma Gz(t - \tau_1))w(z), \operatorname{sgn}(z)\sqrt{1 - w^2(z)}\big], \tag{10}$$

and therefore

$$\boldsymbol{M}'(x, y, z; \tau_1) = Cb_0\rho(x, y, z)\big[w(z), \operatorname{sgn}(z)\sqrt{1 - w^2(z)}\big]. \tag{11}$$

As has been known since the work of Hahn, we can create spin echoes, even with a permanent field gradient, see [14]. The analysis is only slightly different if the direction of $\widehat{\boldsymbol{B}}_0$ is slowly varying. This leads to small variations in the degree to which the magnetization is refocused which, in turn, produces a slowly varying shading in the reconstructed image.

To measure the total density of spins within the slice we could average the signal over a time interval $[\tau_1 - \tau_{\text{acq}}, \tau_1 + \tau_{\text{acq}}]$ leading to a measured signal of the form

$$\begin{aligned} S_{\text{echo}} &= \frac{C\omega_0^2}{2\tau_{\text{acq}}} \int_{\mathbb{R}^3} b_{\text{rec}\,1}(x, y, z)\rho(x, y, z)w(z) \left[\int_{-\tau_{\text{acq}}}^{\tau_{\text{acq}}} \exp(\mathrm{i}\gamma Gzs)\,\mathrm{d}s\right] \mathrm{d}x\,\mathrm{d}y\,\mathrm{d}z \\ &= C\omega_0^2 \int_{\mathbb{R}^3} \operatorname{sinc}(\gamma Gz\tau_{\text{acq}}) b_{\text{rec}\,1}(x, y, z)\rho(x, y, z)w(z)\,\mathrm{d}x\,\mathrm{d}y\,\mathrm{d}z. \end{aligned} \tag{12}$$

Here we assume that $\tau_{\text{acq}} \leqslant \tau_1$. Supposing that G is large, and Δz is the width of the excited slice, the requirement that $\operatorname{sinc}(\gamma Gz\tau_{\text{acq}})$ remain positive throughout the excited slice leads to a maximum reasonable value for τ_{acq}:

$$\tau_{\text{acq}} \leqslant \frac{\pi}{\Delta f} \qquad \text{where} \quad \Delta f = \gamma G\Delta z. \tag{13}$$

Since the length of the time interval over which the signal is averaged effectively determines the bandwidth of the measured signal, we see that, in inhomogeneous field imaging, the size of the permanent gradient effectively determines the minimum 'receiver bandwidth'. We return to this observation in section 4.

We now turn to step 4, the encoding of spatial information. From (10) it is apparent that the phase of the transverse magnetization is marching inexorably forwards. This suggests a *stroboscopic* approach to signal acquisition. By combining gradients with refocusing pulses we could sample the Fourier transform of ρ. How often this procedure can be repeated is largely determined by the size of T_2, and how well the magnetization can be repeatedly refocused. If the permanent gradient is large, then diffusion effects might also lead to a rapid decay of signal strength. This approach to the problem has been considered by several groups of investigators. For the most part, the previous work uses pulsed gradients for spatial encoding, and refocusing pulses to repeatedly refocus the accumulating phase in the direction of the permanent gradient. These ideas are described in the 1987 patent of Bendel, see [2], as well as a 1989 patent of Cho and Wong, see [3]. The idea is further developed by Crowley and Rose as described in their 1994 and 1996 patents, see [6] and [5]. As far as I know, this line of investigation is not described in the ordinary research literature. Pulsed gradients are also used in SPRITE, though for different reasons, see [1].

Crowley and Rose make the important observation that a large permanent gradient leads to a rapid traversal of $\boldsymbol{k}$-space and a short refocusing time. So that, within the time constraints imposed by transverse relaxation, many samples can be collected. On the other hand, a large gradient means that to excite a reasonably sized slice requires a large RF-bandwidth and thereby an increased SAR. Indeed, as a refocusing pulse is required for each point sampled in $\boldsymbol{k}$-space, these imaging sequences have a much larger SAR than most sequences used with homogeneous fields. In section 4 we examine how SNR and SAR requirements limit the ratio $\|\nabla\|\widehat{\boldsymbol{B}}_0\|\|/\|\widehat{\boldsymbol{B}}_0\|$.

We now briefly describe an alternative approach to the problem of spatial encoding and signal acquisition, which uses a single refocusing pulse per *line* in $\boldsymbol{k}$-space. As this technique leads to irregularly spaced samples, we must use a technique like regridding to obtain regularly spaced samples, before we can reconstruct an image; see [8, 22].

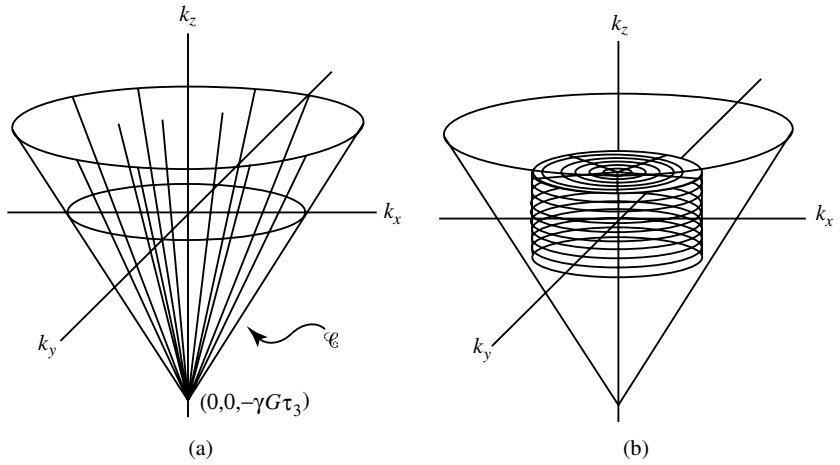

Figure 4. Indications of the region of $\boldsymbol{k}$-space sampled by the direct 3D method. (a) The cone $\mathscr{C}$, which contains the samples points for $\mathscr{F}(\overline{\rho})$, showing some lines along which samples are acquired. (b) The cylinder, $\mathscr{K}$, within $\mathscr{C}$, in which the sample points for the regridded data lie.

After the selective excitation, the magnetization is allowed to freely precess for an additional τ_2 units of time so that, after a refocusing pulse, the magnetization is given by

$$\boldsymbol{M}(x, y, z) = Cb_0\rho(x, y, z)\big[\exp(-\mathrm{i}\gamma Gz\tau_3)w(z), \operatorname{sgn}(z)\sqrt{1 - w^2(z)}\big], \quad (14)$$

where $\tau_3 = \tau_1 + \tau_2$. At this point, a gradient of the form

$$\boldsymbol{B}_{\mathrm{fe}\,0} = (g_x, g_y, 0) \cdot (x, y, z)\hat{\boldsymbol{z}}$$

is turned on. If t is normalized so that the end of the refocusing pulse occurs at $t = 0$, then the transverse magnetization is given, for $t \geqslant 0$, by

$$M_{xy}(x, y, z; t) = Cb_0\rho(x, y, z)\exp(\mathrm{i}\gamma[Gz(t - \tau_3) + t(g_x x + g_y y)])w(z). \quad (15)$$

Sampling at times $t \in \{j\Delta t : j = 0, \ldots, N\}$ we measure approximate values for $\{\mathscr{F}(\overline{\rho})(j\Delta k_x, j\Delta k_y, j\Delta k_z - k_{z\max})\}$, where

$$\overline{\rho}(x, y, z) = 2C\omega_0^2 \operatorname{sinc}(\gamma Gz\tau_{\mathrm{acq}})\rho(x, y, z)b_{1\,\mathrm{rec}}(x, y, z)w(z), \quad (16)$$

and

$$\Delta k_x = \gamma g_x \Delta t, \qquad \Delta k_y = \gamma g_y \Delta t, \qquad \Delta k_z = \gamma G\Delta t. \quad (17)$$

By adjusting the coefficients of the gradient field, $\boldsymbol{B}_{\mathrm{fe}\,0}$, we can obtain samples of $\mathscr{F}(\overline{\rho})$ along straight lines lying within a cone, $\mathscr{C}$, with vertex at $(0, 0, -\gamma G\tau_3)$, see figure 4(a). By regridding we can then obtain samples of $\mathscr{F}(\overline{\rho})$ which are uniformly spaced on a cylindrical grid, lying inside a cylinder, $\mathscr{K}$ contained within the cone $\mathscr{C}$, see figure 4(b). An image could then be reconstructed by using the standard Fourier transform in the z-direction and a filtered backprojection algorithm in the transverse plane. For the filtered backprojection algorithm see [8].

To use a method like regridding requires a certain amount of oversampling. For each sample point p_j on the regular grid within $\mathscr{K}$, severally irregularly spaced samples must be collected in a neighbourhood of p_j. It is also clear that samples from near the vertex of $\mathscr{C}$ may not be usable in the regridding process. Additionally, the samples become rather

spread out as we cross the $k_z = 0$ plane. It may be preferable to measure $\mathscr{F}(\overline{\rho})(\boldsymbol{k})$, for $\boldsymbol{k}$ with nonpositive k_z, and recover the values in the other half plane using the symmetry $\mathscr{F}(\overline{\rho})(-\boldsymbol{k}) = \mathscr{F}(\overline{\rho})(\boldsymbol{k})^*$. It is clear that there are many possible variations on this general approach to spatial encoding. For example, one might begin with a larger τ_3 and a large initial gradient to first move the vertex of the cone to (k_{x0}, k_{y0}, k_{z0}). After reducing the gradient, samples could then be collected along a line of the form $(k_{x0}, k_{y0}, k_{z0}) + t\gamma(g_x, g_y, G)$.

3. Inhomogeneous fields without critical points: 2

We now consider the general case of imaging with an inhomogeneous field without critical points. As before, the permanent gradient in the background field is used as a slice select gradient. Several investigators have obtained partial results in this direction. See, for example, [11], [17], or [23]. In these papers the analysis is either perturbative, or done with unnecessarily restrictive hypotheses on the background field or the gradients. In this section, we give minimal hypotheses on the background and gradient fields under which the measurements can, after a change of variables in physical space, be interpreted as samples of the ordinary Fourier transform.

Remark 3 (Notational conventions)**.** We suppose that the object being imaged lies in a region of space that we denote by D. We refer to D as the *field of view*. The object is described by a density function $\rho(x, y, z)$, supported in D. As usual $\widehat{\boldsymbol{B}}_0$ denotes the background field.

(1) For much of the remainder of the paper we let

$$\phi_0(x, y, z) = \|\widehat{\boldsymbol{B}}_0(x, y, z)\|,$$

and suppose it takes values in $[c_0, c_1]$, for points lying in D. The *local Larmor frequency* at (x, y, z) is $\gamma\phi_0(x, y, z)$.

(2) If f is a real valued function defined in a region D, then for each $c \in \mathbb{R}$

$$f^{-1}(c) = \{(x, y, z) \in D : \ f(x, y, z) = c\}.$$

Our initial assumptions concern the function $\phi_0(x, y, z)$:

(1) The function $\phi_0(x, y, z)$ has no critical points within the field of view. This means that the level sets,

$$\mathscr{S}_{\gamma c} = \{(x, y, z) \in D : \ \phi_0(x, y, z) = c\} \tag{18}$$

are smooth. The level sets are labelled by the local Larmor frequency.

(2) We assume that the coordinates (x, y, z) are chosen so that each level set $\mathscr{S}_{\gamma c}$ can be represented as a graph over a (fixed) region R in the (x, y)-plane. In other words, there is a smooth function $z(x, y, c)$ so that $\phi_0(x, y, z(x, y, c)) = c$ for $c \in [c_0, c_1]$ and therefore

$$\mathscr{S}_{\gamma c} = \{(x, y, z(x, y, c)) : \ (x, y) \in R\}. \tag{19}$$

With these assumptions, we let the region D be the set

$$D = \{(x, y, z(x, y, c)) : \ (x, y) \in R \text{ and } c \in [c_0, c_1]\},$$

see figure 5. The second assumption is not strictly necessary. Though, without something like it, one cannot expect to use the Fourier transform, in any simple way, to reconstruct the spin density. Indeed the mathematical analysis required becomes vastly more complicated.

We first give a formula for the measured signal without additional gradients, which we later modify to include the effect of gradients. Let ω_0 denote $\gamma\phi_0(0, 0, 0)$, and assume that

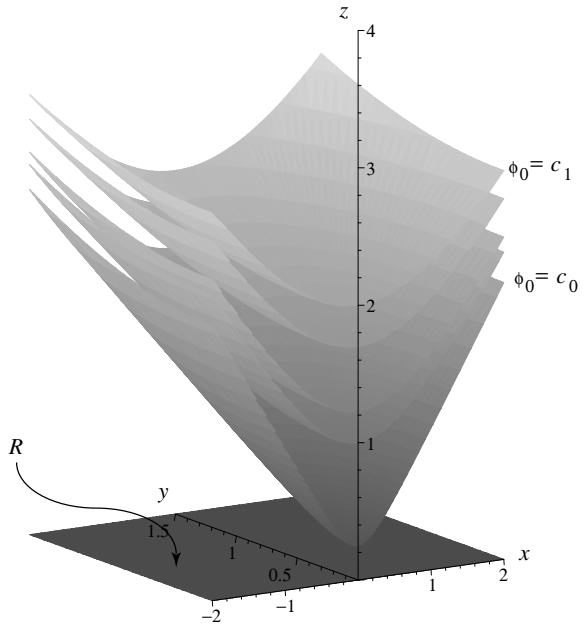

Figure 5. The level surfaces of a nonlinear function, ϕ_0, which can be represented as graphs over region R.

$[\omega_0 - \Delta\omega, \omega_0 + \Delta\omega]$ is contained in $[\gamma c_0, \gamma c_1]$. Suppose that the polarized sample is irradiated with a selective RF-pulse designed to flip spins lying in the region where the local Larmor frequency lies between $\omega_0 - \Delta\omega$ and $\omega_0 + \Delta\omega$. We describe this in terms of an excitation profile $w(\phi_0)$. For example, an ideal 90° flip has excitation profile given by

$$w_{90}(c) = \begin{cases} 1 & \text{for} \quad \gamma c \in [\omega_0 - \Delta\omega, \omega_0 + \Delta\omega] \\ 0 & \text{for} \quad \gamma c \notin [\omega_0 - \Delta\omega, \omega_0 + \Delta\omega]. \end{cases} \tag{20}$$

After the initial RF-pulse, the signal as a function of time is given by

$$S_0(t) = C\gamma \int_D \rho(x, y, z) b_{\mathrm{rec}\,1}(x, y, z) \phi_0^2(x, y, z) w(\phi_0(x, y, z)) \exp(\mathrm{i}\gamma\phi_0(x, y, z)t)\, \mathrm{d}x\, \mathrm{d}y\, \mathrm{d}z. \tag{21}$$

One factor of $\phi_0(x, y, z)$ comes from the definition of the equilibrium magnetization and the other comes from Faraday's law. Time is labelled so that $t = 0$ corresponds to the spin echo induced by a refocusing pulse as described in the previous section. Using our second assumption we change variables to (x, y, c), obtaining

$$S_0(t) = C\gamma \int_R \left[\int_{c_0}^{c_1} \frac{\rho(x, y, c) b_{\mathrm{rec}\,1}(x, y, c)}{\partial_z \phi_0(x, y, z(x, y, c))} c^2 w(c) \exp(\mathrm{i}\gamma c t)\, \mathrm{d}c \right] \mathrm{d}x\, \mathrm{d}y. \tag{22}$$

The denominator in (22) is computed using the chain rule. It is the Jacobian of the transformation $(x, y, z) \to (x, y, c)$. To simplify the notation we use $\rho(x, y, c)$ and $b_{\mathrm{rec}\,1}(x, y, c)$ to denote $\rho(x, y, z(x, y, c))$ and $b_{\mathrm{rec}\,1}(x, y, z(x, y, c))$, respectively.

As in section 2, demodulating and averaging $S_0(t)$ over a sufficiently small time interval $[-\tau_{\mathrm{acq}}, \tau_{\mathrm{acq}}]$ gives

$$\bar{S}(0) = C\gamma \int_R \left[\int_{c_0}^{c_1} \frac{\rho(x, y, c) b_{\mathrm{rec}\,1}(x, y, c)}{\partial_z \phi_0(x, y, z(x, y, c))} w(c)\, \mathrm{sinc}(\tau_{\mathrm{acq}}(\gamma c - \omega_0)) c^2\, \mathrm{d}c \right] \mathrm{d}x\, \mathrm{d}y. \tag{23}$$

If $\Delta\omega$ is small enough then we have

$$\bar{S}(0) \approx C' \int_R \frac{\rho(x, y, \gamma^{-1}\omega_0) b_{\mathrm{rec}\,1}(x, y, \gamma^{-1}\omega_0)}{\partial_z \phi_0(x, y, z(x, y, \gamma^{-1}\omega_0))}\, \mathrm{d}x\, \mathrm{d}y. \tag{24}$$

Up to a scale factor, this is the total spin density along the slice $\mathscr{S}_{\omega_0}$, weighted by $b_{\mathrm{rec}\,1}/\partial_z\phi_0$.

We now consider the addition of gradients to resolve the three-dimensional structure of ρ. As in the previous section, we use a scheme that directly samples a three-dimensional Fourier transform. Because the direction of $\widehat{\boldsymbol{B}}_0$ varies, we need to consider the properties of the actual gradient fields, and not simply their projections along a fixed direction. For our discussion we imagine that we can generate gradient fields in the region D, which can be represented as linear combinations of two *basic gradient fields*. We denote the basic gradient fields by $\boldsymbol{G}_1$ and $\boldsymbol{G}_2$. They are solutions, defined in a neighbourhood of D, of the time-independent vacuum Maxwell equation.

In order to do imaging in a straightforward manner we require two assumptions about the gradient fields:

(3) For all pairs (η_1, η_2) satisfying $|\eta_j| \leqslant \eta_{\max}$, $j = 1, 2$, we can generate the field $\eta_1\boldsymbol{G}_1 + \eta_2\boldsymbol{G}_2$.

(4) For each $c \in [c_0, c_1]$, the map from R to a subset of the plane, defined by

$$\begin{aligned} X &= \boldsymbol{G}_1(x, y, z(x, y, c)) \cdot \widehat{\boldsymbol{B}}_0(x, y, z(x, y, c))/c, \\ Y &= \boldsymbol{G}_2(x, y, z(x, y, c)) \cdot \widehat{\boldsymbol{B}}_0(x, y, z(x, y, c))/c, \end{aligned} \tag{25}$$

is one-to-one and has a smooth inverse.

In standard imaging, with a background field given by $\widehat{\boldsymbol{B}}_0 = (0, 0, b_0)$, the basic gradient fields are modelled as $\boldsymbol{G}_1 = (z, 0, x)$ and $\boldsymbol{G}_2 = (0, z, y)$. It is well known that we can generate the linear combinations described in assumption 3. In this case $X = x$, $Y = y$, so both assumptions are easily seen to be satisfied.

Remark 4. Due to the linear nature of Maxwell's equations, if, using electromagnets, we can generate the fields $\boldsymbol{G}_1$ and $\boldsymbol{G}_2$, in the region D, then, by adjusting the currents, we can also generate the linear combinations called for in assumption 1. In and of itself, condition 3 is essentially a triviality. It is also *the* fundamental requirement for obtaining data that can be interpreted as samples of the Fourier transform of a function simply related to ρ.

Condition 4 is a bit harder to check in practice. If the direction of $\widehat{\boldsymbol{B}}_0$ does not vary too much over the region D, then this condition is also easily satisfied. Let us suppose that $\{\tilde{\boldsymbol{x}}, \tilde{\boldsymbol{y}}, \tilde{\boldsymbol{z}}\}$ is an orthonormal frame such that $\widehat{\boldsymbol{B}}_0(0, 0, 0)$ is parallel to $\tilde{\boldsymbol{z}}$. It is easy to show that there are vacuum solutions of Maxwell's equations of the form

$$\boldsymbol{G}_1 = x\tilde{\boldsymbol{z}} + a_1\tilde{\boldsymbol{x}} + a_2\tilde{\boldsymbol{y}}, \qquad \boldsymbol{G}_2 = y\tilde{\boldsymbol{z}} + a_2\tilde{\boldsymbol{x}} + b_2\tilde{\boldsymbol{y}}, \tag{26}$$

where a_1, a_2, b_1, b_2 are linear functions, vanishing at $(0, 0, 0)$. With these solutions we see that

$$X = x + \text{h.o.t.}, \qquad \mathrm{Y} = \mathrm{y} + \text{h.o.t.},$$

here h.o.t. are terms vanishing quadratically at $(0, 0, 0)$. Hence, if the field of view is not too large, or alternately, the direction of $\widehat{\boldsymbol{B}}_0$ does not vary too rapidly, then the pair (X, Y), defined by the fields given in (26), satisfies assumption 4.

We now see how the expression for the signal is modified by the addition of the gradient fields. It is assumed that ϕ_0 is sufficiently large throughout the field of view so that we can ignore components of $\boldsymbol{G}_1$ and $\boldsymbol{G}_2$ orthogonal to $\widehat{\boldsymbol{B}}_0$. Here we use a spatial encoding scheme

like that described in section 2. For each allowable pair (η_1, η_2) we have an expression for the signal:

$$S_{(\eta_1,\eta_2)}(t) \approx \frac{C\omega_0^2}{\gamma} \int_{\mathbb{R}^2} \left[\int_{c_0}^{c_1} \frac{\rho(x, y, c) b_{\mathrm{rec}\,1}(x, y, c)}{\partial_z \phi_0(x, y, z(x, y, c))} \times w(c) \exp(\mathrm{i}\gamma[c(t - \tau_3) + t\eta_1 X(x, y, c) + t\eta_2 Y(x, y, c))]) \, \mathrm{d}c \right] \mathrm{d}x \, \mathrm{d}y. \quad (27)$$

The time parameter is normalized so that the refocusing pulse ends at $t = 0$, at which time the gradient field $\eta_1 \boldsymbol{G}_1 + \eta_2 \boldsymbol{G}_2$ is switched on.

Using assumption 2, we can solve for $x(X, Y, c)$ and $y(X, Y, c)$ throughout the region of integration. Let $J(X, Y, c)$ denote the Jacobian of this change of variables: $\mathrm{d}x \, \mathrm{d}y = J(X, Y, c) \, \mathrm{d}X \, \mathrm{d}Y$. The expression for the signal becomes

$$S_{(\eta_1,\eta_2)}(t) \approx \frac{C\omega_0^2}{\gamma} \int_{c_0}^{c_1} \left[\int_{\mathbb{R}^2} \overline{\rho}(X, Y, c) w(c) \exp(\mathrm{i}\gamma[c(t - \tau_3) + t(\eta_1 X + \eta_2 Y)]) \, \mathrm{d}X \, \mathrm{d}Y \right] \mathrm{d}c \quad (28)$$

where

$$\overline{\rho}(X, Y, c) = \frac{\rho(x(X, Y, c), y(X, Y, c), c) b_{\mathrm{rec}\,1}(x(X, Y, c), y(X, Y, c), c)}{\partial_z \phi_0(x(X, Y, c), y(X, Y, c), z(x(X, Y, c), y(X, Y, c), c))} J(X, Y, c). \quad (29)$$

Demodulating and sampling we measure samples $\mathscr{F}(w\overline{\rho})(\boldsymbol{k}_j)$, where, as before, the points $\{\boldsymbol{k}_j\}$ lie along straight lines within $\mathscr{C}$. The normalization here is a little different from that used in the previous section. In the earlier case, with $\widehat{\boldsymbol{B}}_0$ given by equation (5), we did not need to change variables in the 'z-direction'.

We see that, up to a constant, the measured signal equals the ordinary Fourier transform of $w\overline{\rho}(X, Y, c)$. Using regridding and filtered backprojection, we can therefore reconstruct $w\overline{\rho}(X, Y, c)$. To determine the original spin density requires a knowledge of $b_{1\,\mathrm{rec}}$ and the transformations $(x, y, z) \leftrightarrow (x, y, c) \leftrightarrow (X, Y, c)$. These in turn can be computed with a knowledge of the background field $\widehat{\boldsymbol{B}}_0$ and the basic gradient fields $\boldsymbol{G}_1$ and $\boldsymbol{G}_2$. The necessary coordinate transformations are determined by the fields $\widehat{\boldsymbol{B}}_0$, $\boldsymbol{G}_1$ and $\boldsymbol{G}_2$, which means that they can be computed once and stored. But for the need to do this reparametrization before displaying the image, the computational requirements for imaging with an inhomogeneous field are comparable to those found in x-ray CT. Measurements could equally well be made using refocusing pulses and stroboscopic acquisition as described in the previous section. Though, if the direction of the background field varies significantly within the field of view, then, as the refocusing errors accumulate, this approach might suffer additional signal loss.

The conditions above on the background field and gradient fields are essentially that the functions

$$\phi_0(x, y, z), \qquad \frac{\boldsymbol{G}_1(x, y, z) \cdot \widehat{\boldsymbol{B}}_0(x, y, z)}{\phi_0(x, y, z)}, \qquad \frac{\boldsymbol{G}_2(x, y, z) \cdot \widehat{\boldsymbol{B}}_0(x, y, z)}{\phi_0(x, y, z)}, \quad (30)$$

define a one-to-one map from the field of view to a set of the form $[c_0, c_1] \times R$, with R a subset of $\mathbb{R}^2$. Implicitly, we have also assumed that the direction of $\widehat{\boldsymbol{B}}_0$ does not vary too much within D. We need this assumption in order to apply the analysis of selective excitation with an inhomogeneous background field presented in appendix A. In this case we also expect the receive coil sensitivity, $b_{\mathrm{rec}\,1}$, to be approximately constant (or at least bounded from below) within D. Under these conditions we see that the size of the measured signal obtainable with an inhomogeneous field should be comparable to the signal that can be obtained with a homogeneous field. Because there is always a large gradient, diffusion effects may also diminish the signal.

4. Limits on field inhomogeneity

In this section, we suppose that $\widehat{\boldsymbol{B}}_0$ is an inhomogeneous field without critical points, so that, as in the previous two sections, the permanent gradient serves as the slice select gradient. The basic method for quantifying the quality of measured data is through the signal-to-noise ratio. Generally speaking, the signal strength can be increased by increasing either the background field strength or the thickness of the slice. For a given slice select gradient, the thickness of the slice is proportional to the bandwidth of the RF-excitation. In medical applications, the limits on the allowable specific absorption rate (SAR) of RF-energy constrain the maximum allowable bandwidth. The precise dependence of SAR on the details of the experimental set-up and the frequency of the excitation is an active field of research. In this section we use standard models for SNR and SAR to obtain bounds on the size of the relative field inhomogeneity usable in medical applications. We use the simple model for $\widehat{\boldsymbol{B}}_0$ given in (5), though it is clear that a similar analysis applies in any situation where the 'slice select' gradient remains on throughout the experiment.

Let Δz denote the thickness of the excited slice. The RF-bandwidth needed to excite the slice is given by

$$\Delta f_{\text{trans}} \approx \gamma G \Delta z. \tag{31}$$

On the other hand, we saw in section 2 that the minimum receiver bandwidth is essentially determined by the field gradient. According to equation (13) we have

$$\Delta f_{\text{rec}} = \frac{\pi}{\tau_{\text{acq}}} \geqslant \gamma G \Delta z. \tag{32}$$

For our SNR computation we compare the strength of the measured signal at $\boldsymbol{k} = 0$ with the noise, assuming that the dominant source of noise is Johnson noise caused by the sample itself.

The formula for the signal as a function of time, with no additional gradients or spatial encoding, is

$$S(t) = \frac{\gamma \hbar^2 \omega_0^2}{4kT} \int_{\text{Sample}} \rho'(x, y, z) b_{\text{rec}\,1}(x, y, z) w(z) \exp(\mathrm{i}\gamma G z t)\, \mathrm{d}x\, \mathrm{d}y\, \mathrm{d}z. \tag{33}$$

Here $\omega_0 = \gamma b_0$, T is the absolute temperature of the sample, $w(z)$ is the slice selection profile, and $b_{\text{rec}\,1}$ is the sensitivity function of the receive coil. For simplicity we assume that ρ' and $b_{\text{rec}\,1}$ are constants, ρ_0 and $b_{\text{rec}\,1}$, respectively, and

$$w(z) = \begin{cases} 1 & \text{for} \quad z \in [-\Delta z/2, \Delta z/2] \\ 0 & \text{for} \quad z \notin [-\Delta z/2, \Delta z/2]. \end{cases}$$

Let A denote the cross sectional area of the sample where $w(z) = 1$. With these assumptions, the signal measured, using the maximum value of τ_{acq} (minimum receiver bandwidth), consistent with (32) is

$$\bar{S} = \frac{1}{2\tau_{\text{acq}}} \int_{-\tau_{\text{acq}}}^{\tau_{\text{acq}}} S(t)\, \mathrm{d}t, \tag{34}$$

which gives

$$\begin{aligned} \bar{S} &= \frac{\gamma \hbar^2 \omega_0^2 \rho_0 b_{\text{rec}\,1} A}{8kT\tau_{\text{acq}}} \int_{-\tau_{\text{acq}}}^{\tau_{\text{acq}}} \int_{-\Delta z/2}^{\Delta z/2} \exp(\mathrm{i}\gamma G z t)\, \mathrm{d}z\, \mathrm{d}t \\ &= \frac{\hbar^2 \omega_0^2 \rho_0 b_{\text{rec}\,1} A I}{4kT\tau_{\text{acq}} G}, \end{aligned} \tag{35}$$

where

$$I = \int_{-\pi}^{\pi} \frac{\sin t \, \mathrm{d}t}{t} \approx 3.704.$$

Using the relation $\tau_{\mathrm{acq}} G = \pi(\gamma \Delta z)^{-1}$, the last line in (35) can be rewritten as

$$\bar{S} = \frac{\hbar^2 \omega_0^2 \rho_0 b_{\mathrm{rec}\,1} A I \gamma \Delta z}{4\pi k T}. \tag{36}$$

We now derive an expression for the noise. The RMS noise is given by Nyquist's formula:

$$V_N = \sqrt{4kT R(\omega) \Delta f_{\mathrm{rec}}}, \tag{37}$$

here $R(\omega)$ is the effective resistance. Hoult and Lauterbur show that

$$R(\omega) = \sqrt{\alpha a^2 \omega^{1/2} + \beta b_{\mathrm{rec}\,1}^2 V_s^{5/3} \omega^2}, \tag{38}$$

see [16]. Here α and β are constants determined by the coil geometry, a is the 'radius' of the detector coil, and V_s is the volume of the sample within the coil. Typical values for α and β are

$$\alpha \approx 10^{-1}, \qquad \beta \approx 2.$$

Assuming that the sample noise dominates, we obtain an expression for the SNR:

$$\mathrm{SNR} \approx \frac{I \gamma \hbar^2 \rho_0 A \omega_0 \Delta z}{\pi \sqrt{(4kT)^3 \beta V_s^{5/3} \Delta f_{\mathrm{rec}}}}. \tag{39}$$

If we let

$$C_{\mathrm{SNR}} = \frac{I \hbar^2 \rho_0 A}{\pi \sqrt{(4kT)^3 \beta V_s^{5/3}}},$$

using (31), this can be rewritten as

$$\mathrm{SNR} = C_{\mathrm{SNR}} \frac{\omega_0 \Delta f_{\mathrm{trans}}}{G \sqrt{\Delta f_{\mathrm{rec}}}}. \tag{40}$$

For a given experimental set-up, there is a positive constant, m_{SNR} so that, in order for the measurements to be usable, it is necessary that the SNR of each measurement exceed m_{SNR}. The lower bound on the SNR of the individual measurements is determined by the required quality of the final image, and the amount of time available to repeat the measurements. Given such a lower bound, equation (40) implies that

$$\frac{G}{\omega_0} \leqslant \frac{C_{\mathrm{SNR}} \Delta f_{\mathrm{trans}}}{m_{\mathrm{SNR}} \sqrt{\Delta f_{\mathrm{rec}}}}, \tag{41}$$

more generally we can rewrite this as

$$\frac{\|\nabla \|\widehat{\boldsymbol{B}}_0\|\|}{\|\widehat{\boldsymbol{B}}_0\|} \leqslant \frac{C_{\mathrm{SNR}}}{m_{\mathrm{SNR}}} \frac{\Delta f_{\mathrm{trans}}}{\sqrt{\Delta f_{\mathrm{rec}}}}. \tag{42}$$

Using the observation that the minimum value for Δf_{rec} is $\Delta f_{\mathrm{trans}}$, we see that

$$\frac{\|\nabla \|\widehat{\boldsymbol{B}}_0\|\|}{\|\widehat{\boldsymbol{B}}_0\|} \leqslant \frac{C_{\mathrm{SNR}}}{m_{\mathrm{SNR}}} \sqrt{\Delta f_{\mathrm{trans}}}. \tag{43}$$

Thus SNR considerations and limitations on RF-bandwidth constrain the size of the maximum relative gradient.

In addition to a lower limit on the SNR, there are also upper limits on the allowable SAR (specific absorption rate). Imaging techniques using stroboscopic acquisition have a very large SAR, compared to standard spin-warp imaging. This is because the measurement of each sample of $\mathscr{F}(\rho)$ requires a refocusing pulse. If an RF-pulse produces a flip angle ψ for offset frequencies in a band of width Δf then, formula (43) in [9] shows that the total energy in the pulse satisfies[1]

$$E_{\psi,\Delta f} \geqslant \frac{4\Delta f}{\pi\gamma^2} \log\left[\frac{2}{1+\cos\psi}\right]. \tag{44}$$

For flip angles close to π, we see that the minimum energy pulse satisfies

$$E_{\psi,\Delta f} \approx \frac{8\Delta f \log[4(\pi-\psi)^{-1}]}{\pi\gamma^2},$$

for example

$$E_{0.99\pi,\Delta f} \approx 12 E_{0.5\pi,\Delta f}.$$

Hence, for the computation of the SAR, using stroboscopic acquisition, we can ignore the initial 90° pulse, and account only for the SAR, which results from the train of refocusing pulses. To compute the SAR we use the formula of Hoult and Lauterbur for the power dissipated in the sample:

$$W(t) = C_{\text{geo}} V_s^{5/3} \sigma \omega_0^2 b_{\text{trans}\,1}^2(t), \tag{45}$$

here σ is the conductivity of the sample, and C_{geo} is a constant, which accounts for the geometry of the coil and the sample; it is of the order of 4, see [16]. To estimate the SAR, we integrate $W(t)$ over one repetition period, and divide by T_R, the repeat time. Assuming that we measure N samples of $\mathscr{F}(\rho)$, this gives

$$\text{SAR} \approx \frac{8C_{\text{geo}} V_s^{5/3} \sigma \omega_0^2 N \Delta f_{\text{trans}} \log[4(\pi-\psi)^{-1}]}{\pi\gamma^2 T_R}. \tag{46}$$

Setting

$$C_{\text{SAR}} = \frac{8C_{\text{geo}} V_s^{5/3} \sigma \log[4(\pi-\psi)^{-1}]}{\pi\gamma^2},$$

this becomes

$$\text{SAR} \approx C_{\text{SAR}} \tau_s \omega_0^2 \Delta f_{\text{trans}}, \tag{47}$$

where $\tau_s = N/T_R$. These formulae are only valid at reasonably low frequencies; recent numerical computations indicate that, for ω_0 exceeding about 100 MHz, the ω_0^2 power law should, perhaps, be replaced by ω_0^α for an α closer to 1, see [12, 15]. The linear dependence on Δf_{trans} should nonetheless persist so long as $\Delta f_{\text{trans}} \ll \omega_0$. The upper limit on the allowable SAR implies that there is constant M_{SAR} such that

$$\tau_s \omega_0^2 \Delta f_{\text{trans}} \leqslant \frac{M_{\text{SAR}}}{C_{\text{SAR}}}. \tag{48}$$

Combining (42) with (48) shows that

$$\frac{\|\nabla\|\widehat{\boldsymbol{B}}_0\|\|}{\|\widehat{\boldsymbol{B}}_0\|} \leqslant \sqrt{\frac{M_{\text{SAR}}}{\tau_s C_{\text{SAR}}}} \frac{C_{\text{SNR}}}{m_{\text{SNR}}\omega_0}. \tag{49}$$

[1] In most MR literature it is stated that the energy of a selective pulse is proportional to the square of the flip angle. This is only approximately true for small flip angles. The formulae given here follow from an exact formula, given in [9, 21], for the minimum energy required to flip the magnetization through an angle ψ, for offset frequencies lying in a band of length Δf.

Given an upper bound on the SAR, and a lower bound on the SNR, the maximum allowable relative gradient decreases as the strength of the background field increases. As noted above, the actual rate of decrease is probably closer to $O\left(\omega_0^{-\alpha/2}\right)$, for an α close to 1.

For the three-dimensional acquisition technique, described in section 2, to be usable, it is probably necessary to excite a rather wide slice. This in turn calls for a large Δf_{trans}. To analyse this situation we use

$$\text{SAR} \approx \frac{\widetilde{C}_{\text{SAR}}\omega_0^2\Delta f_{\text{trans}}}{T_R}, \tag{50}$$

where, in this case,

$$\widetilde{C}_{\text{SAR}} = \frac{8C_{\text{geo}}V_s^{5/3}\sigma(\log(2)+\log[4(\pi-\psi)^{-1}])}{\pi\gamma^2}.$$

This accounts for one 90° pulse and a single refocusing pulse. As before, we have a constant M_{SAR} so that

$$\Delta f_{\text{trans}} \leqslant \frac{T_R M_{\text{SAR}}}{\widetilde{C}_{\text{SAR}}\omega_0^2}, \tag{51}$$

and therefore

$$\frac{\|\nabla\|\widehat{\boldsymbol{B}}_0\|\|}{\|\widehat{\boldsymbol{B}}_0\|} \leqslant \sqrt{\frac{T_R M_{\text{SAR}}}{\widetilde{C}_{\text{SAR}}}}\frac{C_{\text{SNR}}}{m_{\text{SNR}}\omega_0}. \tag{52}$$

In the present instance, the limitation placed on Δf_{trans} by equation (51) may prove to be the more decisive constraint.

5. The geometry of level sets near to a critical point

We now turn our attention to imaging with fields such that $\phi_0(x, y, z)$ has a critical point within the field of view. Our goal is to understand the region in the sample that is excited by a selective RF-pulse. As before we assume that the direction of $\widehat{\boldsymbol{B}}_0$ does not vary too much within the field of view.

Suppose that the pulse excites frequencies in the range $[\omega_0 - \Delta\omega, \omega_0 + \Delta\omega]$. In light of (1) this is the region of the space lying between the two level sets ϕ_0, $\mathscr{S}_{\omega_0-\Delta\omega}$ and $\mathscr{S}_{\omega_0+\Delta\omega}$. In this section we consider the consequences of ϕ_0 having a critical point on the geometry of its level sets. If ϕ_0 does not have critical points, then the level sets all look essentially the same. Indeed the flow defined by the vector field $\frac{\nabla\phi_0}{\|\nabla\phi_0\|}$ maps these level sets onto one another, see figure 5 and [18].

In the neighbourhood of a critical point, the geometry of the level sets of f may change. We consider only *nondegenerate* critical points. A twice differentiable function $f(x, y, z)$ has a nondegenerate critical point at (x_0, y_0, z_0) if

$$\nabla f(x_0, y_0, z_0) = (\partial_x f(x_0, y_0, z_0), \partial_y f(x_0, y_0, z_0), \partial_z f(x_0, y_0, z_0)) = (0, 0, 0), \tag{53}$$

and the Hessian matrix,

$$H_f(x_0, y_0, z_0) = \left.\begin{bmatrix} \partial_x^2 f & \partial_x\partial_y f & \partial_x\partial_z f \\ \partial_y\partial_x f & \partial_y^2 f & \partial_y\partial_z f \\ \partial_z\partial_x f & \partial_z\partial_y f & \partial_z^2 f \end{bmatrix}\right|_{(x,y,z)=(x_0,y_0,z_0),}$$

is invertible. Taylor's formula states that

$$f(x, y, z) = f(x_0, y_0, z_0) + \nabla f(x_0, y_0, z_0)\cdot(x - x_0 + y - y_0 + z - z_0) + \frac{1}{2}(x - x_0, y - y_0, z - z_0)\cdot H_f(x_0, y_0, z_0)\begin{pmatrix} x - x_0 \\ y - y_0 \\ z - z_0 \end{pmatrix} + \text{h.o.t.} \tag{54}$$

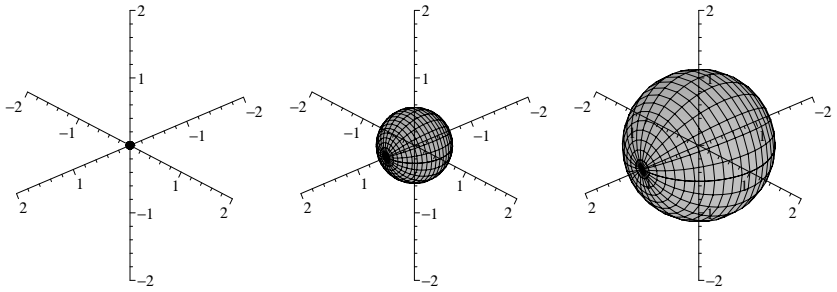

Figure 6. Level surfaces of a function with a nondegenerate critical point such that H_f has all positive eigenvalues. (a) The ν_0 level surface. (b) The $\nu_0 + 0.25$ level surface. (c) The $\nu_0 + 1$ level surface.

Here h.o.t. are terms which vanish at (x_0, y_0, z_0) faster than $(x-x_0)^2+(y-y_0)^2+(z-z_0)^2$. Let $\nu_0 = f(x_0, y_0, z_0)$ be the critical value of f at (x_0, y_0, z_0). Because $\nabla f(x_0, y_0, z_0)$ vanishes and $H_f(x_0, y_0, z_0)$ is invertible, the geometry of the level sets near to $f^{-1}(\nu_0)$ is determined by the second-order term.

It is a consequence of Morse's lemma, see [18], that there is a change of variables $x(X, Y, Z)$, $y(X, Y, Z)$, $z(X, Y, Z)$ defined in a neighbourhood of (x_0, y_0, z_0) such that $(x_0, y_0, z_0) \leftrightarrow (0, 0, 0)$, and, in the (X, Y, Z)-coordinates, the function f takes the form

$$f(X, Y, Z) = \nu_0 + \epsilon_1 X^2 + \epsilon_2 Y^2 + \epsilon_3 Z^2. \tag{55}$$

Here the coefficients $\{\epsilon_1, \epsilon_2, \epsilon_3\}$ are either $+1$ or -1. We call these *Morse coordinates*. Using these coordinates we get rid of the error terms (h.o.t.) in equation (54), and put the quadratic term into a simple form. The only question is how to determine the coefficients $\{\epsilon_j\}$. The matrix $H_f(x_0, y_0, z_0)$ is symmetric and therefore has real eigenvalues. Because it is invertible, no eigenvalue equals zero. There are four cases. If all eigenvalues are positive then $(\epsilon_1, \epsilon_2, \epsilon_3) = (+1, +1, +1)$. If two eigenvalues are positive and one is negative then $(\epsilon_1, \epsilon_2, \epsilon_3) = (+1, +1, -1)$. If one eigenvalue is positive and two are negative then $(\epsilon_1, \epsilon_2, \epsilon_3) = (+1, -1, -1)$. If all eigenvalues are negative then $(\epsilon_1, \epsilon_2, \epsilon_3) = (-1, -1, -1)$.

In the first case f has a local minimum at (x_0, y_0, z_0); in the second and third cases, f has a saddle point at (x_0, y_0, z_0); in the last case f has a local maximum at (x_0, y_0, z_0). In figures 6–9 we show level sets of f near to (x_0, y_0, z_0), in Morse coordinates, for each of these cases. Note that in cases 1 and 4 the level set $f^{-1}(\nu_0)$ consists of a single point, and the nearby level sets are spheres. In cases 2 and 3 the level set $f^{-1}(\nu_0)$ is a cone, and the nearby level sets are hyperboloids of either one or two sheets.

In applications to magnetic resonance imaging $f = \gamma \|\boldsymbol{B}_0(x, y, z)\|$, where $\boldsymbol{B}_0$ is a static vacuum solution to Maxwell's equation. In this case it is not possible for H_f to have all negative eigenvalues at a critical point; this is because Δf is the trace of the matrix H_f, and $\Delta f \geqslant 0$.

It is easy to see, from examples, that the function $\phi_0(x, y, z)$ can have an isolated critical point while, at the same time, the direction of $\widehat{\boldsymbol{B}}_0$ varies very little in a neighbourhood of the critical point. As noted before, this means that the usual theory of selective RF-excitation applies in this case as well. Suppose that the pulse excites frequencies in the range $[\omega_0 - \Delta\omega, \omega_0 + \Delta\omega]$. Here ω_0 is a critical value of $\gamma\phi_0(x, y, z)$. We assume that $\Delta\omega$ is

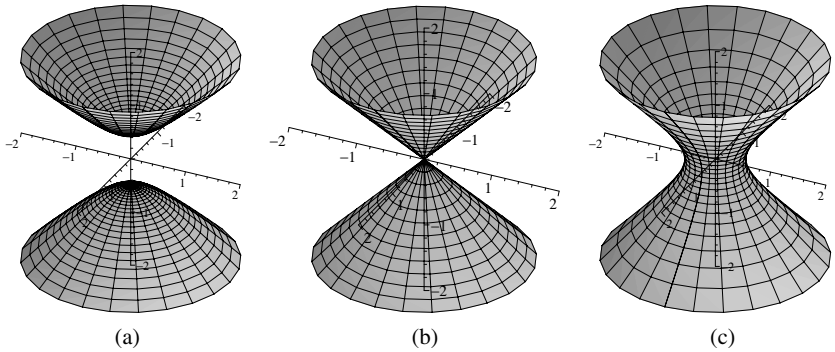

(a) (b) (c)

Figure 7. Level surfaces of a function with a nondegenerate critical point such that H_f has two positive eigenvalues and one negative eigenvalue. (a) The $\nu_0 - 0.25$ level surface. (b) The ν_0 level surface. (c) The $\nu_0 + 0.25$ level surface.

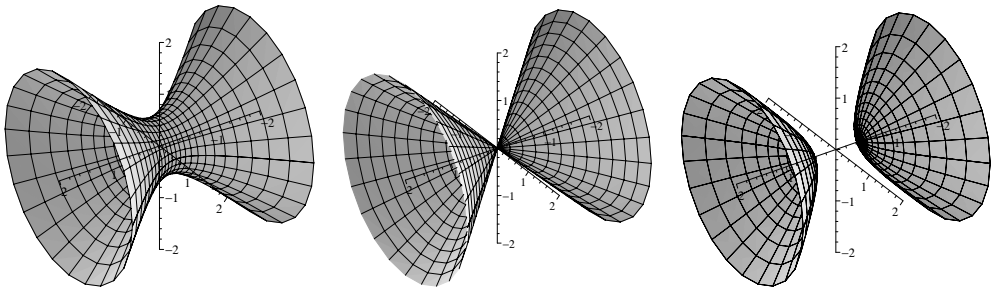

(a) (b) (c)

Figure 8. Level surfaces of a function with a nondegenerate critical point such that H_f has one positive eigenvalue and two negative eigenvalues. (a) The $\nu_0 - 0.25$ level surface. (b) The ν_0 level surface. (c) The $\nu_0 + 0.25$ level surface.

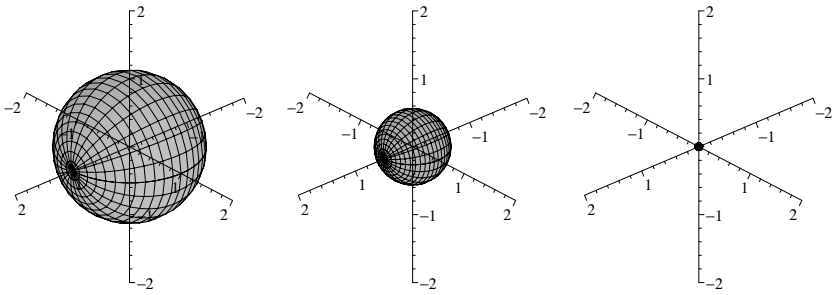

(a) (b) (c)

Figure 9. Level surfaces of a function with a nondegenerate critical point such that H_f has all negative eigenvalues. (a) The $\nu_0 - 1$ level surface. (b) The $\nu_0 - 0.25$ level surface. (c) The ν_0 level surface.

sufficiently small so that ϕ_0 has no other critical points in field of view. The selective pulse excites the region

$$\{(x, y, z) : \omega_0 - \Delta\omega \leqslant \gamma\phi_0(x, y, z) \leqslant \omega_0 + \Delta\omega\}.$$

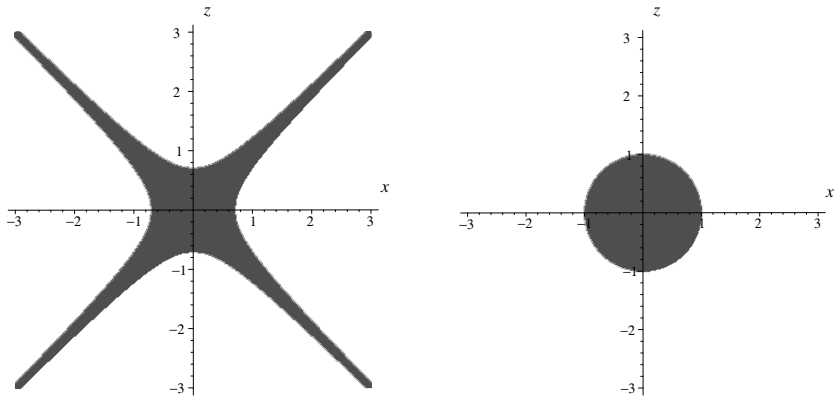

(a) (b)

Figure 10. Cross sectional views showing the regions of space excited by selective pulses centred on a critical value of ϕ_0. In all cases the region of space is axially symmetric. In (a) if H_f has $2+$ eigenvalues and $1-$ then the z-axis is the axis of symmetry, with $1+$ eigenvalue and $2-$ the x-axis is the axis of symmetry. (a) Saddle point; (b) minimum.

Since a physical $\boldsymbol{B}$-field decays to zero at infinity, the level surfaces of ϕ_0 are closed bounded sets. Hence, Morse coordinates are only valid in a bounded subset. In the analyses which follow, we assume that Morse coordinates are valid throughout the region occupied by the sample.

In figure 10 we show cross sections of the excited regions. In Morse coordinates these are axially symmetric regions. If ϕ_0 has a saddle point, then the regions are as depicted in figure 10(a). This is essentially an *unbounded* region. On the other hand, if ϕ_0 has a local minimum, then the excited region, shown in figure 10(b), is the bounded region enclosed by the level surface

$$\mathscr{S}_{\omega_0+\Delta\omega} = \{(X, Y, Z) : \gamma\phi_0(X, Y, Z) = \omega_0 + \Delta\omega\}.$$

6. Fields with saddle points

We now consider the difficulties one encounters in attempting to image or do localized spectroscopy, with a field such that ϕ_0 has a saddle-type critical point. Such an approach has been used in the FONAR and TOPICAL techniques. In this section the time parameter t is normalized so that the echo occurs at $t = 0$.

The underlying principle behind using a background field with a critical point is that the spins dephase more rapidly in a field with a strong gradient. Hence, *for large times*, the main contribution to the measured signal derives from the part of the sample located close to the critical point. This is indeed true. In the mathematics and physics literature, this observation goes under the name of the *principle of stationary phase*, see [10]. On the other hand, as we shall show, the short time signal is mostly produced by regions of the sample quite distant from the critical point. This means that the data are only spatially localized near to the critical point for large times, when the signal has largely decayed.

We recall the statement of the principle of stationary phase.

Theorem 1 (principle of stationary phase)**.** *Suppose that f and g are smooth functions defined on $\mathbb{R}^3$. Suppose that g has bounded support, and that, on the support of g, f has a single*

nondegenerate critical point (at $\mathbf{0} = (0, 0, 0)$ *for the sake of definiteness). If* f *is real valued and* $g(\mathbf{0}) \neq 0$*, then, as* t *tends to infinity, we have the asymptotic formula:*

$$\int_{\mathbb{R}^3} \exp(\mathrm{i}tf(x, y, z))g(x, y, z)\,\mathrm{d}x\,\mathrm{d}y\,\mathrm{d}z \sim \frac{2\pi \exp\left(\frac{\pi \mathrm{i}\,\mathrm{sgn}H_f(\mathbf{0})}{4}\right)\exp(\mathrm{i}tf(\mathbf{0}))g(\mathbf{0})}{\sqrt{t^3|\det H_f(\mathbf{0})|}}\left[1 + \sum_{j=1}^{\infty}\frac{a_j}{t^j}\right], \tag{56}$$

here

$$\operatorname{sgn} H_f(\mathbf{0}) = \#\{+\textit{eigenvalues of } H_f(\mathbf{0})\} - \#\{-\textit{eigenvalues of } H_f(\mathbf{0})\}.$$

The coefficients $\{a_j\}$ *depend on the derivatives of* f *and* g *evaluated at* $\mathbf{0}$*.*

Formula (56) shows that the signal decays like $t^{-3/2}$. This rapid decay leads to a significantly diminished SNR for the spatially localized part of the FID. The failure of spatial localization, in the case of a saddle point, for the small time part of the signal, is a consequence of the following simple geometric lemma.

Lemma 1. *For positive real numbers* μ *and* ν*, the volume of the region of space*

$$\mathscr{R}_{\mu,\nu} = \{(x, y, z) : -\mu^2 \leqslant x^2 + y^2 - z^2 \leqslant \mu^2 \textit{ and } \mu \leqslant z \leqslant \mu + \nu\}$$

is given by

$$\operatorname{Vol}(\mathscr{R}_{\mu,\nu}) = 2\pi\nu\mu^2. \tag{57}$$

Suppose ϕ_0 has a saddle-type critical point at $\mathbf{0}$; introduce Morse coordinates (X, Y, Z), so that, in a neighbourhood of $\mathbf{0}$, ϕ_0 takes the form

$$\phi_0(X, Y, Z) = \frac{\omega_0}{\gamma} + X^2 + Y^2 - Z^2.$$

At least for points fairly close to $\mathbf{0}$, the change of variables $(x, y, z) \to (X, Y, Z)$ has the effect of scaling volumes by a positive constant, C_V. A selective excitation flips the spins in a region of space, given in the (X, Y, Z)-coordinates by

$$\mathscr{R}_{\mu} = \{(X, Y, Z) : -\mu^2 \leqslant X^2 + Y^2 - Z^2 \leqslant \mu^2\}.$$

For the purposes of this discussion, the points in $\mathscr{R}_{\mu}$ 'close' to $\mathbf{0}$ are taken to be those for which $|Z| \leqslant \mu$. This region is denoted by $\mathscr{R}_{\text{close}}$. The volume of $\mathscr{R}_{\text{close}}$ is

$$\operatorname{Vol}(\mathscr{R}_{\text{close}}) = \tfrac{8}{3}\pi\mu^3.$$

From the lemma it follows that

$$\frac{\operatorname{Vol}(\mathscr{R}_{\mu,\nu})}{\operatorname{Vol}(\mathscr{R}_{\text{close}})} = \frac{3}{4}\frac{\nu}{\mu}. \tag{58}$$

If the sample has approximately constant spin density, then, equation (58) shows that the part of the $t = 0$ signal, coming from points close to the critical point, is approximately equal to that coming from $\mathscr{R}_{\mu,\frac{4}{3}\mu}$. More generally, the signal coming from $\mathscr{R}_{\mu,\frac{4m}{3}\mu}$ is m times the signal coming from $\mathscr{R}_{\text{close}}$. This verifies our assertion that, for times close to the echo time, the vast majority of the measured signal comes from parts of the sample quite distant from the critical point. This is the essential difficulty in using a field with a saddle point for imaging or localized spectroscopy. In [24] a technique employing two RF-pulses is given that produces spatially localized spectroscopic data using gradient fields with saddle-type critical points.

7. Fields with local minima

If one could create a magnetic field $\widehat{\boldsymbol{B}}_0$ such that $\|\widehat{\boldsymbol{B}}_0(x, y, z)\|$ assumes an isolated minimum value, then one could measure localized spectroscopic data using a single RF-pulse. Suppose the minimum occurs at (x_0, y_0, z_0) and $\omega_0 = \gamma\phi_0(x_0, y_0, z_0)$. A selective excitation which excites frequencies in the band $[\omega_0 - \Delta\omega, \omega_0 + \Delta\omega]$ would only excite spins in the region of space bounded by the *closed* surface

$$\mathscr{S}_{\omega_0+\Delta\omega} = \{(x, y, z) : \gamma\phi_0(x, y, z) = \omega_0 + \Delta\omega\}.$$

The entire FID is then produced by spins lying in a bounded region of space, close to the critical point of ϕ_0. We now give examples of such fields. These fields are obtained as perturbations of a uniform background field

$$\widehat{\boldsymbol{B}}_0 = [0, 0, b_0].$$

For real parameters ϵ and δ we define

$$\boldsymbol{B}_{0,\epsilon\delta} = \widehat{\boldsymbol{B}}_0 + \epsilon[x, -y, 0] + \delta[-2xz, 0, (z^2 - x^2)]. \tag{59}$$

It is an elementary computation to see that

$$\nabla \cdot \boldsymbol{B}_{0,\epsilon\delta} = 0, \qquad \nabla \times \boldsymbol{B}_{0,\epsilon\delta} = 0$$

and therefore these vector fields define vacuum solutions of Maxwell's equations. We compute the length of $\boldsymbol{B}_{0,\epsilon\delta}$

$$\|\boldsymbol{B}_{0,\epsilon\delta}\|^2 = b_0^2 + (\epsilon^2 - 2b_0\delta)x^2 + \epsilon^2 y^2 + 2b_0\delta z^2 - 4\epsilon\delta x^2 z + \delta^2(x^2 + z^2)^2. \tag{60}$$

The function ϕ_0 equals the square root of $\|\boldsymbol{B}_{0,\epsilon\delta}\|^2$, and therefore

$$\nabla\phi_0 = \frac{\nabla\|\boldsymbol{B}_{0,\epsilon\delta}\|^2}{2\|\boldsymbol{B}_{0,\epsilon\delta}\|}.$$

The critical points of ϕ_0, where ϕ_0 does not vanish, therefore agree with the critical points of $\|\boldsymbol{B}_{0,\epsilon\delta}\|^2$. At critical points, where $\phi_0 \neq 0$, the Hessian matrices satisfy

$$H_{\phi_0} = \frac{H_{\|\boldsymbol{B}_{0,\epsilon\delta}\|^2}}{2\|\boldsymbol{B}_{0,\epsilon\delta}\|}. \tag{61}$$

This shows that the types of the critical points agree as well.

From equation (60), it is clear that ϕ_0 has a critical point at $(0, 0, 0)$. The Hessian is a diagonal matrix,

$$H_{\phi_0}(0, 0, 0) = \frac{2}{\phi_0(0, 0, 0)} \begin{bmatrix} \epsilon^2 - 2b_0\delta & 0 & 0 \\ 0 & \epsilon^2 & 0 \\ 0 & 0 & 2b_0\delta \end{bmatrix}. \tag{62}$$

This demonstrates the following result:

Proposition 1. *If $\delta b_0 > 0$ and $\epsilon^2 > 2\delta b_0$, then $\boldsymbol{B}_{0,\epsilon\delta}$ is a vacuum solution of Maxwell's equations such that $\|\boldsymbol{B}_{0,\epsilon\delta}\|$ has an isolated minimum at* $(0, 0, 0)$.

The fields $[x, -y, 0]$ and $[-2xz, 0, z^2 - x^2]$ are essentially standard gradient fields. Therefore $\boldsymbol{B}_{0,\epsilon\delta}$ can be generated by using an arrangement of gradient coils within a standard homogeneous, high field magnet. We will consider the practical problems of generating these fields, and using them for imaging, in a subsequent publication. We close this section with figure 11, showing level surfaces of $\boldsymbol{B}_{0,\epsilon\delta}$ with $b_0 = 1, \epsilon = 0.1, \delta = 0.0025$.

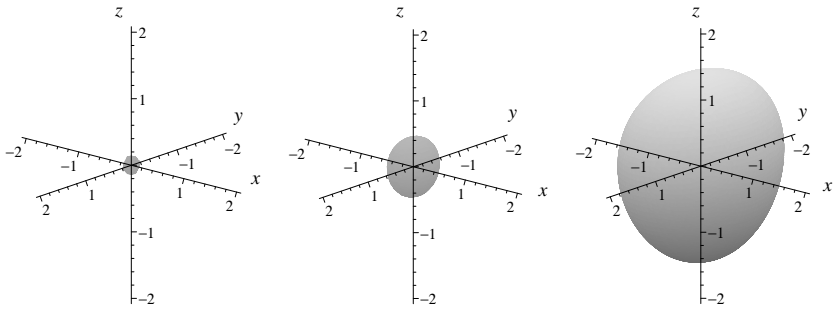

Figure 11. Level surfaces of the length of $\boldsymbol{B}_{0.0.1\times0.0025}$ with $b_0 = 1$. (a) The $\phi_0 = 1.000\,05$ level surface. (b) The $\phi_0 = 1.0005$ level surface. (c) The $\phi_0 = 1.005$ level surface.

8. Conclusion

In the first part of the paper, we show how a magnet producing an inhomogeneous field, without critical points, might be used to produce the background field for an MR-imaging system. In particular, we show that the main difficulty that one encounters with a nonhomogeneous background field is that of refocusing the phase that accumulates along the direction of $\nabla\|\widehat{\boldsymbol{B}}_0\|$. We outline a method for directly sampling the 3D-Fourier transform of ρ. An interesting feature of this analysis is that the size of the permanent field gradient imposes a *lower* bound on the bandwidth of the receiver. The question of the practical limits on field inhomogeneity awaits numerical simulation and experimental verification. In section 4 we showed that considerations of SNR and SAR constrain the size of the allowable relative field gradient $\|\nabla\|\widehat{\boldsymbol{B}}_0\|\|/\|\widehat{\boldsymbol{B}}_0\|$.

We give simple geometric criteria for the MR measurements made, using an inhomogeneous background field and nonlinear gradients, to be samples of the Fourier transform, up to a single change of coordinates. This coordinate change is determined by the background field $\widehat{\boldsymbol{B}}_0$ and the basic gradient fields $\boldsymbol{G}_1, \boldsymbol{G}_2$. As such it need only be computed once and stored. Our computations strongly suggest that it should be possible to obtain a strong signal with a background field having substantial inhomogeneity.

We analyse well-known imaging methods, which employ fields with sweet spots. We show that the principle underlying this approach is nothing other than the classical principle of stationary phase. In all previous works, these sweet spots are of saddle type. We give a simple geometric explanation for the difficulty of obtaining localized information with critical points of this type: when the signal is large, the excited volume of space is seen to be highly nonlocalized. Hence, it is only in the long time limit, when the signal has largely decayed, that spatially localized information is available. We construct examples of fields such that $\|\widehat{\boldsymbol{B}}_0\|$ has an isolated, nonzero local minimum. Using such a field one can obtain a well-localized excitation *ab initio* thereby avoiding the most serious pitfall of earlier approaches to imaging with a sweet spot.

Acknowledgments

I would like to thank Felix Wehrli for inviting me to visit the LSNI, encouraging me to explore inhomogeneous field imaging, and write this paper. He very kindly read early versions of this paper and provided many suggestions for improvements. I would like to thank Peter Joseph

for his perspective on fields with critical points. I would also like to thank Dr David Hoult and the referees of earlier versions of this paper for their many useful suggestions and references. This research was partially supported by NSF grants DMS99-70487 and DMS02-07123, and the Francis J Carey term chair.

Appendix A. RF-pulses in inhomogeneous fields

In this appendix, we examine the effect of a selective RF-pulse in an inhomogeneous background field. We let $\hat{\boldsymbol{x}}, \hat{\boldsymbol{y}}, \hat{\boldsymbol{z}}$ denote orthonormal basis vectors for the laboratory frame. Suppose that $\widehat{\boldsymbol{B}}_0$ is given by

$$\widehat{\boldsymbol{B}}_0(x, y, z) = b_0(x, y, z)(\sin\psi\cos\eta\hat{\boldsymbol{x}} + \sin\psi\sin\eta\hat{\boldsymbol{y}} + \cos\psi\hat{\boldsymbol{z}}),$$

where ψ and η depend on (x, y, z). The coordinates are normalized so that $\psi(0, 0, 0) = 0$, and $\omega_0 = \gamma b_0(0, 0, 0)$. The offset frequency f is a function of spatial position given by

$$f(x, y, z) = \gamma(b_0(x, y, z) - b_0(0, 0, 0)). \tag{A.1}$$

The equilibrium magnetization is normalized to have unit length.

For these computations, it is very useful to represent the coordinates of a vector in $\mathbb{R}^3$ with respect to orthonormal bases as a pair $[w, u]$ where $w \in \mathbb{C}$ and $u \in \mathbb{R}$; in this representation the inner product is given by

$$[w_1, u_1] \cdot [w_2, u_2] = \mathrm{Re}(w_1\bar{w}_2) + u_1u_2.$$

For example, the coordinates of $\widehat{\boldsymbol{B}}_0$, with respect to $\{\hat{\boldsymbol{x}}, \hat{\boldsymbol{y}}, \hat{\boldsymbol{z}}\}$ in this representation are

$$b_0(x, y, z)[\exp(\mathrm{i}\eta(x, y, z))\sin\psi(x, y, z), \cos\psi(x, y, z)].$$

If $[w, u]$ are coordinates representing the vector $\mathrm{Re}(w)\tilde{\boldsymbol{x}} + \mathrm{Im}(w)\tilde{\boldsymbol{y}} + u\tilde{\boldsymbol{z}}$, then, in the *local rotating reference frame* (i.e., with respect to $\tilde{\boldsymbol{z}}$), the coordinates of this vector are $[\exp(-\mathrm{i}\omega_0 t)w, u]$. Throughout this appendix, t is a time parameter, which we normalize to equal 0 at the start of the RF-pulse.

We suppose that the selective RF-pulse is of the form

$$\boldsymbol{B}_1 = \mathrm{Re}(\exp(\mathrm{i}\omega_0 t)\alpha(t))\hat{\boldsymbol{x}} + \mathrm{Im}(\exp(\mathrm{i}\omega_0 t)\alpha(t))\hat{\boldsymbol{y}}.$$

In other words, the RF-pulse is assumed to be spatially independent and orthogonal to the laboratory z-direction, $\hat{\boldsymbol{z}}$. To analyse the effect of $\boldsymbol{B}_1$ on spins located at (x, y, z), we introduce a new orthonormal basis $\{\tilde{\boldsymbol{x}}, \tilde{\boldsymbol{y}}, \tilde{\boldsymbol{z}}\}$ for $\mathbb{R}^3$:

$$\begin{aligned}
\tilde{\boldsymbol{x}} &= \cos\psi\cos\eta\hat{\boldsymbol{x}} + \cos\psi\sin\eta\hat{\boldsymbol{y}} - \sin\psi\hat{\boldsymbol{z}},\\
\tilde{\boldsymbol{y}} &= -\sin\eta\hat{\boldsymbol{x}} + \cos\eta\hat{\boldsymbol{y}},\\
\tilde{\boldsymbol{z}} &= \sin\psi\cos\eta\hat{\boldsymbol{x}} + \sin\psi\sin\eta\hat{\boldsymbol{y}} + \cos\psi\hat{\boldsymbol{z}}.
\end{aligned} \tag{A.2}$$

In (A.2), and throughout the remainder of this appendix, the angles ψ and η are evaluated at (x, y, z). The local $\boldsymbol{z}$-direction, $\tilde{\boldsymbol{z}}$, is parallel to $\widehat{\boldsymbol{B}}_0(x, y, z)$.

We re-express $\boldsymbol{B}_1$ in terms of the basis in (A.2):

$$\begin{aligned}
\boldsymbol{B}_1 = \cos\psi\,&\mathrm{Re}(\alpha(t)\exp(\mathrm{i}(\omega_0 t - \eta)))\tilde{\boldsymbol{x}} + \mathrm{Im}(\alpha(t)\exp(\mathrm{i}(\omega_0 t - \eta)))\tilde{\boldsymbol{y}}\\
&+ \sin\psi\,\mathrm{Re}(\alpha(t)\exp(\mathrm{i}(\omega_0 t - \eta)))\tilde{\boldsymbol{z}}.
\end{aligned}$$

The coordinates of $\boldsymbol{B}_1$ in the local rotating reference frame are

$$\begin{aligned}
\boldsymbol{B}_1 = \frac{(1 + \cos\psi)}{2}&[\alpha(t)\,\mathrm{e}^{-\mathrm{i}\eta}, 0] - \frac{(1 - \cos\psi)}{2}[\bar{\alpha}(t)\exp(-\mathrm{i}(2\omega_0 t + \eta)), 0]\\
&+ \sin\psi[0, \mathrm{Re}(\alpha(t)\exp(\mathrm{i}(\omega_0 t - \eta)))].
\end{aligned} \tag{A.3}$$

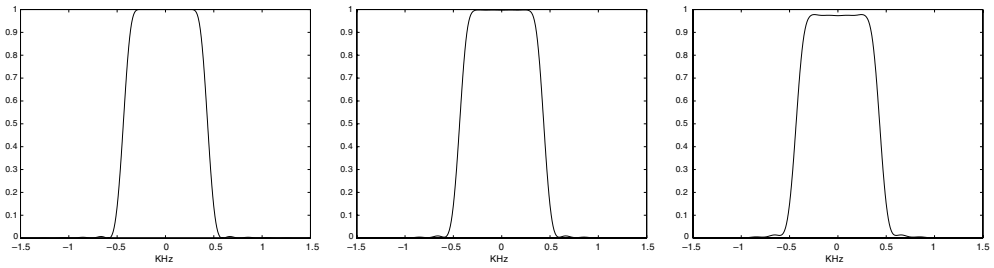

(a) (b) (c)

Figure 12. The absolute values of the transverse component of the magnetization which result from attenuating a minimum energy, $\frac{\pi}{2}$-pulse. Though the flip angle is diminished, the excited slice is almost unchanged. (a) 100%, (b) 95%, (c) 85%.

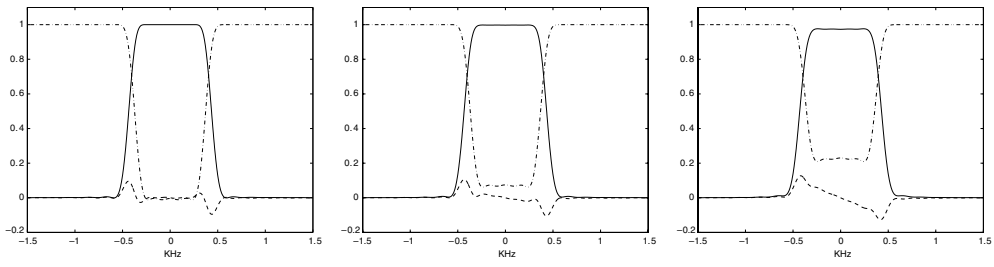

(a) (b) (c)

Figure 13. The magnetization profiles which result from attenuating a minimum energy, $\frac{\pi}{2}$-pulse. The solid line is the $\hat{\boldsymbol{x}}$-component, the dashed line, the $\hat{\boldsymbol{y}}$-component and the dot-dash line the $\hat{\boldsymbol{z}}$-component. (a) 100%, (b) 95%, (c) 85%.

For angles, ψ not too far from 0, the second and third terms have very little effect on the solution of the Bloch equation. First of all their coefficients, $\frac{(1-\cos\psi)}{2}$, $\sin\psi$, are small for small values of ψ. Perhaps more importantly, each is highly oscillatory and, therefore, over the duration of the RF-pulse their effects average to zero. Hence the coordinates of the *effective* $\boldsymbol{B}_1$-field at (x, y, z), in the local rotating reference frame, are

$$\boldsymbol{B}_1 \approx \frac{(1+\cos\psi)}{2}[\alpha(t)\,\mathrm{e}^{-\mathrm{i}\eta}, 0]. \tag{A.4}$$

This shows that the main consequence of having a background field, with slowly varying direction, is a slight attenuation of the effective $\boldsymbol{B}_1$-field. The apparent phase shift in the RF, $\mathrm{e}^{-\mathrm{i}\eta}$, is an artefact of representing the field with respect to $\tilde{\boldsymbol{x}}$, $\tilde{\boldsymbol{y}}$, $\tilde{\boldsymbol{z}}$.

In figure 12 we show the effects on the flip-angle profile of diminishing the amplitude of a minimum energy, selective $\frac{\pi}{2}$-pulse. From the graphs it is apparent that, though the flip angle is diminished, the attenuation hardly affects the selectivity of the pulse. The magnetization profiles, shown in figure 13, indicate that attenuation also leads to an approximately linear phase error in the transverse magnetization. In the following computation, we model the effect of the pulse given in (A.4), as a $\frac{\pi(1+\cos\psi)}{4}$ flip in-slice, with a phase error, at offset frequency f, of the form $\exp(\mathrm{i}\chi(\psi)f)$, and as having no effect, out-of-slice, on the equilibrium magnetization. Here $\chi(\psi)$ is a smooth function vanishing at 0.

Let $\boldsymbol{B}_1$ be a $\frac{\pi}{2}$-pulse with passband $[f_{\min}, f_{\max}]$ and rephasing time τ. If the direction of the field were uniform, then the magnetization at the end of the pulse, before rephasing, would be given, in the laboratory rotating frame, by

$$\boldsymbol{M}_{(x,y,z)} = \begin{cases} [\exp(\mathrm{i} f(x, y, z)\tau), 0] & \text{for} \quad f \in [f_{\min}, f_{\max}], \\ [0, 1] & \text{for} \quad f \notin [f_{\min}, f_{\max}]. \end{cases} \tag{A.5}$$

If the direction of $\widehat{\boldsymbol{B}}_0$ varies but $\psi(x, y, z)$ remains reasonably close to zero, then it follows from (A.4) and our assumptions above, that the effect of this RF pulse, on the spins located at (x, y, z), before rephasing, is given, in the *laboratory* rotating frame, by

$$\boldsymbol{M}_{(x,y,z)} \approx$$
$$\begin{cases} \frac{(1+\cos\psi)}{2}[\exp(\mathrm{i} f(\tau + \chi(\psi))), 0] - \frac{(1-\cos\psi)}{2}[\exp(-\mathrm{i}[2\omega_0 t + f(\tau + \chi(\psi)) - 2\eta]), 0] \\ \quad + \mathrm{Re}(\exp(\mathrm{i}[\omega_0 t + f(\tau + \chi(\psi)) - \eta]))[0, -\sin\psi] \qquad \text{for} \quad f \in [f_{\min}, f_{\max}], \\ [\sin\psi\, \mathrm{e}^{\mathrm{i}\eta}, \cos\psi] \qquad \text{for} \quad f \notin [f_{\min}, f_{\max}]. \end{cases} \tag{A.6}$$

The functions f and ψ are evaluated at (x, y, z). Out of slice, the magnetization remains parallel to $\widehat{\boldsymbol{B}}_0$, while in-slice, the magnitude of the principal transverse component (the $(1+\cos\psi)/2$-term) is slightly reduced. As asserted above, this would produce a slowly varying shading in the reconstructed image. The second transverse component (the $(1-\cos\psi)/2$-term) is quite small for ψ close to zero. Note also the global phase $\exp(-2\mathrm{i}\omega_0 t)$; in formula (A.6), t is the time at the conclusion of the RF-pulse. As this phase factor indicates, this is a counterrotating term, which, when demodulated with quadrature detection, is at frequency $-2\omega_0$. Hence this component can easily be filtered out in the receiver electronics.

Appendix B. Critical points in fields with symmetry

In section 7 we constructed vacuum solutions to Maxwell's equations such that the magnitude of the field has an *isolated* local minimum. In this appendix, we show that an isolated local minimum is not possible under various symmetry hypotheses. First we consider translationally invariant fields. In this case we see that local minima can occur, which, due to the translational invariance, must occur along a line. Next we show that an axially symmetric field cannot have an isolated minimum. Again, because of the axial symmetry, such an isolated minimum would have to occur along the axis of symmetry.

B.1. Translational symmetry

Suppose that $\boldsymbol{B}$ is a translationally invariant field, and that $\boldsymbol{B}$ is independent of the z-coordinate. Hence

$$\boldsymbol{B} = [a(x, y), b(x, y), c(x, y)].$$

For a field of this type, Maxwell's equations read

$$\begin{aligned} &\nabla \times \boldsymbol{B} = 0: \quad \partial_x b - \partial_y a = 0, \quad \partial_x c = \partial_y c = 0, \\ &\nabla \cdot \boldsymbol{B} = 0: \quad \partial_x a + \partial_y b = 0. \end{aligned} \tag{B.1}$$

Evidently c is a constant and the complex valued function $F(x, y) = a(x, y) - \mathrm{i}b(x, y)$ is analytic, i.e., it is a function of the complex variable $z = x + \mathrm{i}y$. From this we conclude that

$$\|\boldsymbol{B}\|^2 = c^2 + |F(z)|^2. \tag{B.2}$$

Equation (B.2) shows that the gradient of $\|\boldsymbol{B}\|^2$ only vanishes at points, z_0, where $F'(z_0)\overline{F(z_0)}$ vanishes. Hence either $F(z_0)$ vanishes or $F'(z_0)$ vanishes. If $F(z_0) = 0$ then z_0 is a local minimum. If $F'(z_0) = 0$, but $F(z_0) \neq 0$, then $|F(z)|^2$ must have a saddle point at z_0.

B.2. Axial symmetry

We now turn to fields with axial symmetry. For definiteness we suppose that the z-axis is the axis of symmetry, and that there are no current sources in a neighbourhood of the z-axis. A field $\boldsymbol{B}(x, y, z)$ has axial symmetry if for every rotation

$$\rho_\theta = \begin{bmatrix} \cos\theta & -\sin\theta \\ \sin\theta & \cos\theta \end{bmatrix}$$

we have

$$\boldsymbol{B}(x\cos\theta - y\sin\theta, x\sin\theta + y\cos\theta, z) = \begin{bmatrix} \rho_\theta & 0 \\ 0 & 1 \end{bmatrix} \boldsymbol{B}. \tag{B.3}$$

Since $\boldsymbol{B}$ is a vacuum solution to Maxwell's equation, we can write $\boldsymbol{B} = \nabla u$, for a harmonic function $u(x, y, z)$. The condition in equation (B.3) is equivalent to the requirement that, for all θ,

$$u(x\cos\theta - y\sin\theta, x\sin\theta + y\cos\theta, z) = u(x, y, z). \tag{B.4}$$

If we set

$$x = r\cos\phi, \qquad y = r\sin\phi,$$

then u is independent of ϕ. This implies that there exists a function $v(r, z)$ so that

$$u(x, y, z) = v\big(\sqrt{x^2 + y^2}, z\big).$$

The equation $\Delta u = 0$ implies that

$$Lv = r\big(\partial_r^2 v + \partial_z^2 v\big) + \partial_r v = 0. \tag{B.5}$$

The field is expressed in these coordinates as

$$\boldsymbol{B} = \left[\frac{x\partial_r v}{\sqrt{x^2 + y^2}}, \frac{y\partial_r v}{\sqrt{x^2 + y^2}}, \partial_z v \right],$$

and therefore

$$\|\boldsymbol{B}\|^2 = (\partial_r v)^2 + (\partial_z v)^2. \tag{B.6}$$

The fact that there are no current sources along the z-axis implies that v is actually a real analytic function of r^2 and z in a neighbourhood of the real axis, hence, we have a convergent power series expansion:

$$v(r, z) = \sum_{j,k=0}^{\infty} a_{jk} r^{2j} z^k. \tag{B.7}$$

Our assertion that $\|\boldsymbol{B}\|$ cannot have a minimum along the z-axis follows by analysing the polynomial solutions of equation (B.5).

Lemma 2. *For each nonnegative integer j there is a unique polynomial in $p_j(r, z)$, homogeneous of degree j, such that*

(1) $p_j(r, z) = z^j + \cdots$.
(2) $Lp_j = 0$.

Proof. The lemma follows from the observation that L commutes with ∂_z. If p is a homogeneous polynomial of degree j which solves $Lp = 0$ then $\partial_z p$ is a homogeneous polynomial of degree $j-1$ which solves $L(\partial_z p) = 0$. The lemma follows once we show that a homogeneous polynomial solution of $Lp = 0$, such that $\partial_z p = 0$, is constant. A homogeneous polynomial p of degree j, with the property that $\partial_z p = 0$, is of the form cr^j. Observe that

$$Lr^j = j^2 r^{j-1}.$$

Thus if $Lr^j = 0$, then $j = 0$. □

The first few polynomials are

$$p_0 = 1, \qquad p_1 = z, \qquad p_2 = z^2 - \tfrac{1}{2}r^2, \qquad p_3 = z^3 - \tfrac{3}{2}r^2 z. \tag{B.8}$$

It is not difficult to show that only even powers of r arise, and that the coefficients alternate in sign. In fact we do not need this sort of precise information, for we observe that $p_j\big(\sqrt{x^2+y^2}, z\big)$ is a homogeneous harmonic polynomial of degree j defined on $\mathbb{R}^3$.

Without loss of generality we can assume that the critical point of $\|\boldsymbol{B}\|$ occurs at $(0, 0, 0)$. The function $v(r, z)$ has an expansion of the form

$$v(r, z) = a_0 + a_1 p_1 + \sum_{j=j_0}^{\infty} a_j p_j(r, z),$$

where $j_0 \geqslant 2$, and $a_{j_0} \neq 0$. It follows from equation (B.6) that

$$\|\boldsymbol{B}\|^2 = a_1^2 + 2a_1 a_{j_0} \partial_z p_{j_0} + a_{j_0}^2 \big(\partial_r p_{j_0}\big)^2 + \text{h.o.t.} \tag{B.9}$$

From this formula, and the fact that $\partial_z p_{j_0}$ is a harmonic function, it is clear that $\|\boldsymbol{B}\|^2$ cannot have a local minimum at $(0, 0, 0)$ unless $a_1 = 0$. In this case $\|\boldsymbol{B}(0, 0, 0)\|^2 = 0$ as well. We have proved the following theorem:

Theorem 2. *Suppose that $\boldsymbol{B}$ is an axially symmetric solution to Maxwell's equations, smooth in a neighbourhood of its axis of symmetry. If $\|\boldsymbol{B}\|$ has an isolated minimum value at a point p, then $\|\boldsymbol{B}\|$ vanishes at p.*

Remark 5. We have not determined whether or not the magnitude of an axially symmetric field can assume a nonzero, minimum value along a circle with r and z constant. This seems unlikely, though the argument given above does not apply to points off the axis of symmetry.

References

[1] Balcom B, MacGregor R, Beyea S, Green D, Armstrong R and Bremner T 1996 Single-point ramped imaging with T_1 enhancement (SPRITE) *J. Magn. Reson.* A **123** 131–4

[2] Bendel P 1987 Method to eliminate the effects of magnetic field inhomogeneities in NMR imaging and apparatus therefor *US Patent 4656425*

[3] Cho Z-H and Wong E K Jr 1991 *Fringe Field MRI* US Patent 5023554

[4] Courant R and Hilbert D 1957 *Methods of Mathematical Physics,* vol 2 (New York: Wiley)

[5] Crowley C W and Rose F H 1996 Method for maintaining encoded coherence for remotely positioned MRI device *US Patent 5493225*

[6] Crowley C W and Rose F H 1994 Remotely positioned MRI device *US Patent 5304930*

[7] Damadian R V 1982 Apparatus and method for nuclear magnetic resonance scanning and mapping *US Patent* 4354499

[8] Epstein C L 2003 *Introduction to the Mathematics of Medical Imaging* (Upper Saddle River, NJ: Prentice-Hall)

[9] Epstein C L 2004 Minimum power pulse synthesis via the inverse scattering transform *J. Magn. Reson.* **167** 185–210

[10] Erdelyi A 1958 *Asymptotic Expansions* (New York: Dover)

[11] Feig E, Greenleaf F and Perlin M 1986 Magnetic resonance imaging with non-uniform fields *Phys. Med. Biol.* **31** 1091–9
[12] Gandhi O P and Chen X B 1999 Specific absorption rates and induced current densities for an anatomy-based model of the human for exposure to time-varying magnetic fields of MRI *Magn. Reson. Med.* **41** 816–23
[13] Gordon R 1982 Topical magnetic resonance *Biosci. Rep.* **2** 701–6
[14] Hahn E 1950 Spin echoes *Phys. Rev.* **80** 580–94
[15] Hoult D 2000 Sensitivity and power deposition in a high field imaging experiment *J. Magn. Reson. Imaging* **12** 46–67
[16] Hoult D and Lauterbur P C 1979 The sensitivity of the zeugmatographic experiment involving human samples *J. Magn. Reson.* **34** 425–33
[17] Lai C 1982 Reconstructing NMR images under magnetic fields with large inhomogeneities *J. Phys. E: Sci. Instrum.* **15** 1093–100
[18] Milnor J 1963 *Morse Theory (Ann. Math. Studies vol 51)* (Princeton, NJ: Princeton University Press)
[19] Pulyer Y M 1998 Planar open magnet MRI system *US Patent* 5744960
[20] Pulyer Y M 1999 Planar open magnet MRI system having active target field shimming *US Patent* 6.002255
[21] Rourke D E and Saunders J K 1995 A simple relationship between total RF pulse energy and magnetization response–the nonlinear generalization of Parseval's relation *J. Magn. Reson.* **115** 189–96
[22] Schomberg H and Timmer J 1995 The gridding method for image reconstruction by Fourier transformation *IEEE J. Med. Imaging* **14** 596–607
[23] Sekihara K, Kuroda M and Kohno H 1984 Image restoration from non-uniform magnetic fields influence for direct Fourier NMR imaging *Phys. Med. Biol.* **29** 15–24
[24] Wu E X, Johnson G, Hilal S K and Cho Z-H 1994 A new 3D localization technique using quadratic field gradients *Magn. Reson. Med.* **32** 242–5